Univerzita Karlova
Přírodovědecká fakulta

Katedra buněčné biologie

Studijní program: Reprodukční a vývojová biologie

Bc. Ondřej Šanovec

LINC complex: The link between chromatin integrity and sperm motility

LINC komplex: Spojník mezi integritou chromatinu a motilitou spermií

Diplomová práce

Vedoucí práce: doc.RNDr. Kateřina Komrsková, Ph.D.

Konzultantka: RNDr. Michaela Frolíková, Ph.D.

Praha 2022

Declaration:

I declare that I have prepared the final thesis independently and that I have stated all used information sources and literature. Neither this work nor a substantial part of it has not been submitted to obtain another or the same academic degree.

In Prague ……. Bc. Ondřej Šanovec …….

Acknowledgment

Here, I would like to express my gratitude to everyone who helped and participated in this thesis. I would like to express my deepest gratitude to Doc., RNDr. Kateřina Komrsková, Ph.D. who gave me the opportunity to work on this project and supervised me, helped with experimental designs and provided me with various useful information. Special appreciation goes to RNDr. Michaela Frolíková, Ph.D. and Mgr. Lukáš Děd, Ph.D. for help with hands-on laboratory work, troubleshooting, statistics and much more. I am also thankful to Attila Juhász who prepared all paraffine blocks for me and also to Ing. Jiří Černý who helped with Lighsheet microscopy. I would like to appreciate my classmates and coworkers Monika Vlčková, Hana Pavlová and Kateřina Bajerová for creating a friendly working environment, psychological support and all the snacks we have shared. Thanks should also go to Veronika Páleníková, Daniela Spěváková, Eliška Valášková and all other members of the laboratory for creating a great working environment and giving me valuable recommendations.

Lastly, I would like to mention Nadace Nadání Josefa, Marie a Zdeňky Hlávkových, for founding my flight tickets to the United States for the 54th annual meeting of the Society for the Study of the Reproduction in December 2021 in St. Louis, USA. Thanks to this money support I was able to travel there and present a poster with preliminary results of this thesis. Thank you!

This thesis is part of the grant GAČR: GC20-20217J, Komrsková: LINC komplex spermií: Spojník mezi integritou chromatinu, motilitou spermií a plodností mužů. 2020-2022.

Abstract

The LINC complex (Linker of the Nucleoskeleton and Cytoskeleton) is a protein structure located in the nuclear membrane that connects the cytoskeleton with the nucleoskeleton. This complex can be found in every mammalian cell including the gametes. However, here the LINC complex is more diverse and less studied than in the somatic cells. In this thesis, the LINC complex and its role in spermiogenesis have been studied in wild-type and Protamine 2 knockout (*Prm2*$^{-/-}$) mice. Protamines are small proteins that replace histones during spermiogenesis. The mouse model generated by the group of prof. Hubert Schorle has a deletion in *Prm2* in exon 1 and its sperm possess a surprising phenotype including complete loss of motility.

Therefore, it was hypothesized that the LINC complex might be responsible for miscommunication between the sperm head and tail which leads to the loss of sperm motility. Results from this study suggest that the LINC complex is not influenced by *Prm2* deletion, however, actin dynamics, cytoskeletal motor proteins and tubulin acetylase/ histone deacetylase activity might be impaired. *Prm2*$^{-/-}$ sperm have a significantly higher abundance of β-actin compared to the wild type. Next, *Prm2*$^{-/-}$ sperm also show a different pattern of acetylation of α-tubulin but no change in the abundance of this protein.

Moreover, as part of this thesis, the CLARITY protocol for imaging of individual seminiferous tubules was optimized. Thanks to this new approach abnormal acrosome formation was described.

Key words: Cytoskeleton; epigenetics; human; KASH; lamin-B; LBR; LINC-complex; modified histones; mouse; nesprin; nucleoskeleton; protamine; spermatogenesis; sperm; SUN

Abstrakt

LINC komplex (z angl. Linker of the Nucleoskeleton and Cytoskeleton) je multiproteinová struktura nacházející se v jaderné membráně, která propojuje cytoskelet s jaderným skeletem. Jedná se o velmi konzervovaný komplex, který se nachází v každé savčí buňce, včetně gamet. Zde je ovšem LINC komplex velice variabilní a sestává se z různých proteinových partner, které mají specifickou lokalizaci. Zároveň se jedná o oblast, oproti somatickým buňkám, málo prozkoumanou. Tato práce se zabývá rolí LINC komplexu během spermiogeneze na myších modelech. Použit byl divoký typ a myší linie s delecí Protaminu 2 (*Prm2*$^{-/-}$). Protaminy jsou male proteiny, které nahrazují histony během spermiogenese. Myší model použitý v této studii, vytvořený týmem profesora Huberta Schorle, má deleci v exonu 1 genu *Prm2*. Důsledkem této delece mají takto ovlivněné myši překvapivý fenotyp, který zahrnuje úplnou ztrátu motility spermií.

Na základě těchto pozorování byla vytvořena hypotéza, že LINC komplex může být zodpovědný za špatnou komunikaci mezi hlavičkou a bičíkem spermie, což vede ke ztrátě pohyblivosti. Výsledky ovšem naznačují, že LINK komplex není ztrátou *Prm2* ovlivněn. Získaná data ovšem naznačují, že by v *Prm2*$^{-/-}$ spermiích mohla být narušena dynamika aktinu, aktivita cytoskeletálních motorů nebo tubulin acetylázy / histon deacetylázy. Spermie *Prm2*$^{-/-}$ myší mají signifikantně navýšeno množství β-tubulinu oproti kontrole. Zároveň je pozorován rozdíl v lokalizace ale ne v množství α-tubulinu na spermiích pocházejících z *Prm2*$^{-/-}$ myší.

Součástí této práce byl také optimalizace CLARITY protokolu pro mikroskopické zobrazování jednotlivých semenotvorných kanálků. Díky této nové metodě bylo odhaleno chybné formování akrozomu u *Prm2*$^{-/-}$ myší.

Klíčová slova: Cytoskeleton; člověk; epigenetika; histonové modifikace; KASH; lamin-B; LBR; LINC-komplex; myš; nesprin; nukleoskeleton; protamin; spermatogenese; spermie; SUN

Abbreviations

APS	Ammonium persulfate
cAMP	Cyclic adenosine monophosphate
CAPZB	F-actin-capping protein subunit bet
CBB	Coomassie Brilliant Blue
DAPI	2-(4-amidinophenyl)-1H -indole-6-carboxamidine
DMSO	Dimethyl sulfoxide
ER	Endoplasmic reticulum
HDAC	Histone deacetylase
HRP	Horseradish peroxidase
IAM	Inner acrosomal membrane
ICS	Intracytoplasmic injection
ICSI	Intracytoplasmic sperm injection
INM	Inner nuclear membrane
IVF	In vitro fertilization
KASH	Klarsicht, ANC-1, Syne homology
LBR	Lamin B receptor
LINC	Linker of the Nucleoskeleton and Cytoskeleton
LmnB	Lamin B
MAP	Microtubule-associated protein
mRNA	Messenger ribonucleic acid
NPC	Nuclear pore complex
OAM	Outer acrosomal membrane
ONM	Outer nuclear membrane
PKA	Protein kinase A
PNA	Peanut agglutinin
PNS	Perinuclear space
Prm2	Protamine 2
qPCR	quantitative polymerase chain reaction

ROS	Reactive Oxygen Species
RPM	Rounds per minute
RPS2	40S Ribosomal Protein S2
RT	Room temperature
RT-PCR	Reverse transcription polymerase chain reaction
SAXO	Stabilizer of axonemal protein
SDS	Sodium dodecyl sulphate
Sept	Septin
STs	Seminiferous tubules
SUN	Sad1 and UNC-84 homology
TAT	Tubulin acetyltransferase
TEMED	Tetramethylethylendiamine
TESE	Testicular sperm extraction
WT	Wild type

Content

1 Introduction

The nuclear envelope (NE) is a specialized extension of the endoplasmic reticulum (ER) with crucial functions. Not only does it separate cytoplasm from nucleoplasm, thus maintaining the integrity of the genetic material, the NE also acts as a transductor of mechanical and signaling forces, and influences chromatin remodelling, or DNA repair (Burke and Stewart, 2014). This transduction is mediated via the LINC complex - Linker of the Nucleoskeleton and Cytoskeleton (Crisp *et al.* 2006).

As part of the ER, the nuclear envelope is composed of a double membrane and perinuclear space (PNS). The perinuclear space is a uniform, 30-50 nm wide gap between the outer nuclear membrane (ONM) and the inner nuclear membrane (INM). To facilitate the nuclear export and import, these two membranes meet, forming nuclear pore complexes (NPC). Moreover, a layer of lamins can be found just beneath the INM, providing structural support to the NE (Franke *et al.* 1981).

The LINC complex is a transmembrane protein complex that mediates the connection of the cytoskeleton and nucleoskeleton (Crisp *et al.* 2006). This complex is well conserved in eukaryotes including plants, yeast, worms, flies, fish, and mammals. It is also widely expressed in different tissues, where it serves distinct functions (Kim *et al.* 2015). The LINC complex is composed mainly of two types of proteins: SUN domain proteins, which are part of the INM, and KASH domain proteins located in the ONM. SUN meets KASH in the lumen of the nuclear envelope creating a structure that bridges the perinuclear space. On the cytoplasmic side, KASH proteins interact with actin, tubulin and plectin, while SUN proteins interact with the nucleoskeleton and nuclear lamina.

2 Theoretical part

2.1 LINC complex and its function in spermiogenesis

Despite the LINC complex is a very conserved structure, there exist serval types of SUN and KASH domain proteins (description below). There is also a number of LINC-associated proteins. LINC complexes can interact with the cytoskeleton, dynein, kinesin, nucleoskeleton (such as Septins), nuclear lamina, emerin, telomeric parts of chromosomes, and centrosomes. These variable combinations together with various binding partners show that the LINC complex is a species and organ-specific structure (Méjat and Misteli, 2010, Pasch et al., 2015).

SUN proteins are type-II transmembrane proteins, which contain conserved Sad1 and UNC84 domains (Malone *et al*., 1999). The N-terminal end spikes towards the nucleus where it interreacts with the nuclear lamina, chromatin and telomeric ends of meiotic chromosomes (Gurusaran and Davies, 2021). The C-terminal end is oriented towards the PNS. The luminal region of SUN proteins contains a conserved SUN domain which is extended by the coiled-coil domain (Starr and Fridolfsson, 2010). In mammals, there are 5 divergent genes coding SUN proteins: *Sun1* and *Sun2* which are broadly expressed through different cell types performing many different functions, and *Sun* 3, *Sun4* (*Spag4*), and *Sun5* (*Spag4l*). These three genes are specifically expressed in testes (Pasch *et al*., 2015).

In mammals, SUN proteins interact with various nuclear structures possessing a broad spectrum of functions. For example, it was found that SUN1 is essential for the tethering of meiotic telomeres to the NE (Ding *et al*., 2007). SUN2 was shown to interact with proteins Ku70 and Ku80, which involve SUN2 into the DNA damage response (Lei *et al*., 2012). Last but not least it was found in somatic cells, that Sun1 and Sun2 interact with Lamin A, and the localization and presence of SUN domain proteins are essential for the correct positing of KASH proteins (Haque *et al*., 2006).

KASH domain proteins are, as well as SUN proteins, type-II transmembrane proteins named after Klarsicht, Anc-1 and Syne-1 homology. Their N-terminal end is anchored in the cytoplasm, while C-terminus faces towards the lumen of the nuclear membrane. This end is short and has a loosely conserved PPPx domain. In mammals, there were identified five different KASH proteins so far. KASH 2 and 4 were not detected in testicular cells, therefore their detailed description is omitted from this thesis (Göb *et al*., 2010). KASH1 and KASH2 are large actin-binding proteins, KASH3 binds to the plectin which interacts with intermediate

filaments and/or actin. KASH4 binds to the microtubule motors – dynein and/or Kinesin – 1 (Starr, 2011). KASH5 is capable of binding to the dynactin and together with SUN1 creates a meiosis-specific LINC complex (Morimoto *et al*., 2012).

Historically, KASH proteins are also called Nesprins (nuclear envelope spectrin repeats). However, the term "Nesprin" is not ideal, because not all KASH domain proteins have spectrin repeats. Moreover, "Nesprin" refers only to KASH proteins found exclusively in mammals (Starr, 2011). As KASH proteins are found not only in mammals, the term KASH will be used in this thesis.

Mouse sperm contain several LINC complexes with distinct functions and expressions. To make the explanation easier, the complexes will be described based on their localization in haploid cells. As this thesis focuses on spermiogenesis, only the role of the LINC complex in postmeiotic cells will be described. More information about that topic can be found for example in Kmonickova *et al.,* 2020. Simple graphic shoving distribution and interactions of LINC proteins are shown in figure 3.

Spermiogenesis is a postmeiotic process, during which sperm acquire its typical shape. In mice and humans, it is divided into 12 steps which describe how round spermatid is transformed into mature spermatozoon (Oakberg, 1956, Muciaccia *et al*., 2013). During this process, acrosome and tail develop and the DNA condensates. Moreover, sperm reduces its size by releasing a residual cytoplasm and most of the organelles in the form of the cytoplasmic droplet (Plant and Zeleznik, 2015). During spermiogenesis distinct cell types can be described: round spermatid, elongating spermatid, elongated spermatid and maturated spermatozoon.

A crucial role in spermiogenesis plays the cytoskeleton. Not only does it allows intracellular vesicular transport, but it also enables the movement of maturating sperm towards the lumen of the seminiferous tubule. Actin creates a scaffold structure, which supports the movement of

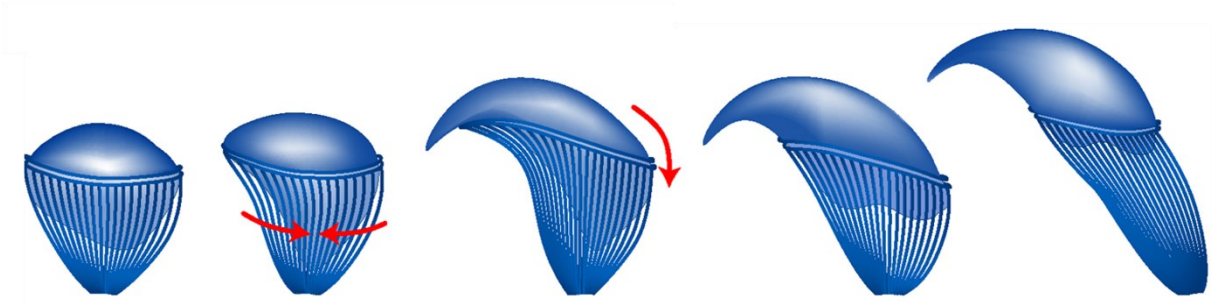

Figure 1: Schematic figure shoving sperm head reshaping through the process of spermiogenesis. The red arrows show the progressive movement of the manchette to the posterior part of the head. This movement mechanically shrinks the sperm head. The figure is taken from (Dunleavy et al.*, 2019).*

cells in the testes. (Romrell and Ross, 1979, Kierszenbaum *et al*., 2011). Another important cytoskeletal structure is the manchette. This is an actomyosin skirt-like structure, that mechanically shrinks the nucleus (Lehti and Sironen, 2016, Dunleavy *et al*., 2019).

The anterior part of the mature mouse sperm contains only one and exceptional LINC complex. It is composed of KASH3 and SUN1η. SUN1η is a shorter splicing variant of SUN1 which lacks exons seven to ten. Therefore, the sequence targeting this protein in the INM is absent. As this is SUN protein, which tends to be incorporated into a membrane, SUN1η is located in the outer acrosomal membrane (OAM). Thanks to the KASH3 capability of binding the actin, this non-nuclear LINC complex has a role in acrosome anchoring via bonding to the acroplaxome. This unique localization suggests, that SUN1η: KASH3 complex has a role in sperm head shaping. Interestingly, SUN1η was also observed in the posterior part of round spermatids. However, with the progression of spermiogenesis, it was gradually relocated to the anterior part of the sperm (Göb *et al*., 2010).

The situation on the posterior part of the sperm is much more complicated. At first, there is a complex made from SUN3, SUN4 and KASH1. Both SUN3 and SUN4 are postmeiotically expressed proteins, which are localized at the lateral posterior part of the spermatid. They were shown to be colocalized with LmnB3 and to have similar properties during sperm maturation. Both proteins are being translocated more and more to the posterior part of the sperm with the progression of the spermiogenesis. However, both SUN proteins, unlike the LaminB3, are

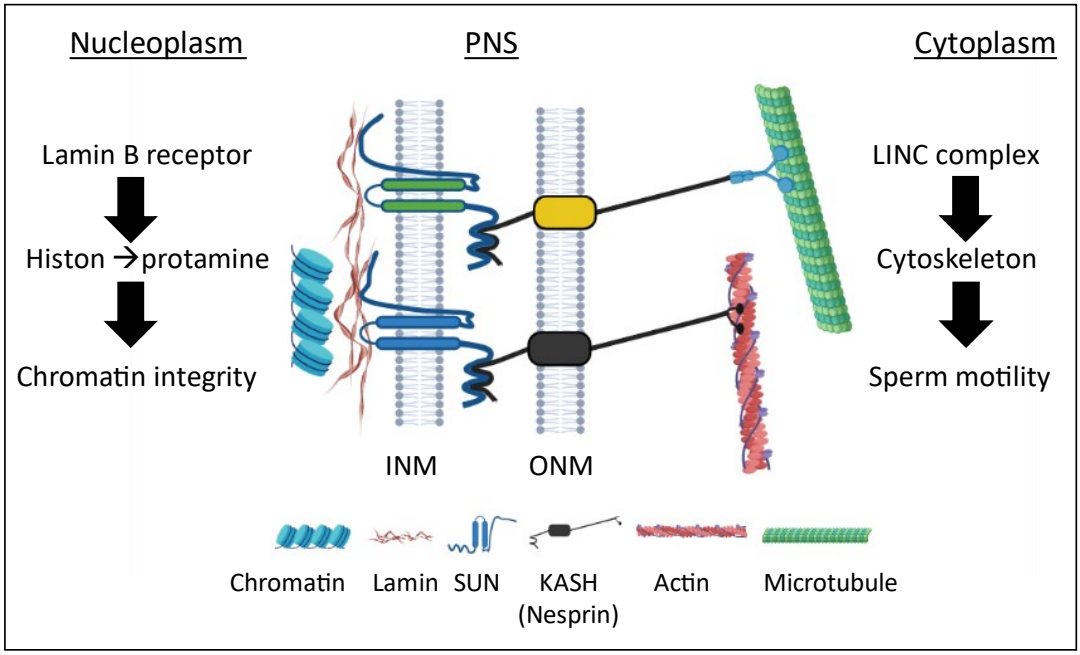

Figure 2: Schematic representation of generic LINC complex in sperm and position in the pathway "From the chromatin to the sperm motility". ONM = outer nuclear membrane, INM = inner nuclear membrane, PNS = perinuclear space. Created in Biorender.com

completely absent from the implementation fossa. In this complex, SUN4 seems to be the one with the essential role. At first, SUN3 has a cytoplasmic domain long only seven amino acids, therefore it is probably not able to bind any nuclear structure. Secondly, it was found on a mouse model where *Sun4* was deleted, that both, SUN3 and KASH1 are mislocalized in the *Sun4*$^{-/-}$ mouse (Pasch *et al*., 2015).

The localization of this complex, its translocation during spermiogenesis and its capability of binding the microtubules, suggest that SUN3 : SUN4 : KASH1 are important for manchette formation (Göb *et al*., 2010, Pasch *et al*., 2015)

The second posterior LINC complex is made from SUN5 and KASH3. KASH3 shows identical localization as SUN1η at the begging of the spermiogenesis. However, KASH3 remains its dual, anterior and posterior, localization. At the posterior part of the spermatid, the KASH3 is located in the head to tail junction, where it interacts with SUN5. It was shown on the *Sun5*$^{-/-}$ mouse model, that SUN5 : KASH3 LINC complex is essential for connecting head to tail. *Sun5*$^{-/-}$ sperm have an acephalic sperm phenotype where the sperm head is fully separated from its tail (Zhang *et al*., 2021). SUN5 is expressed in all stages of spermatogenesis from

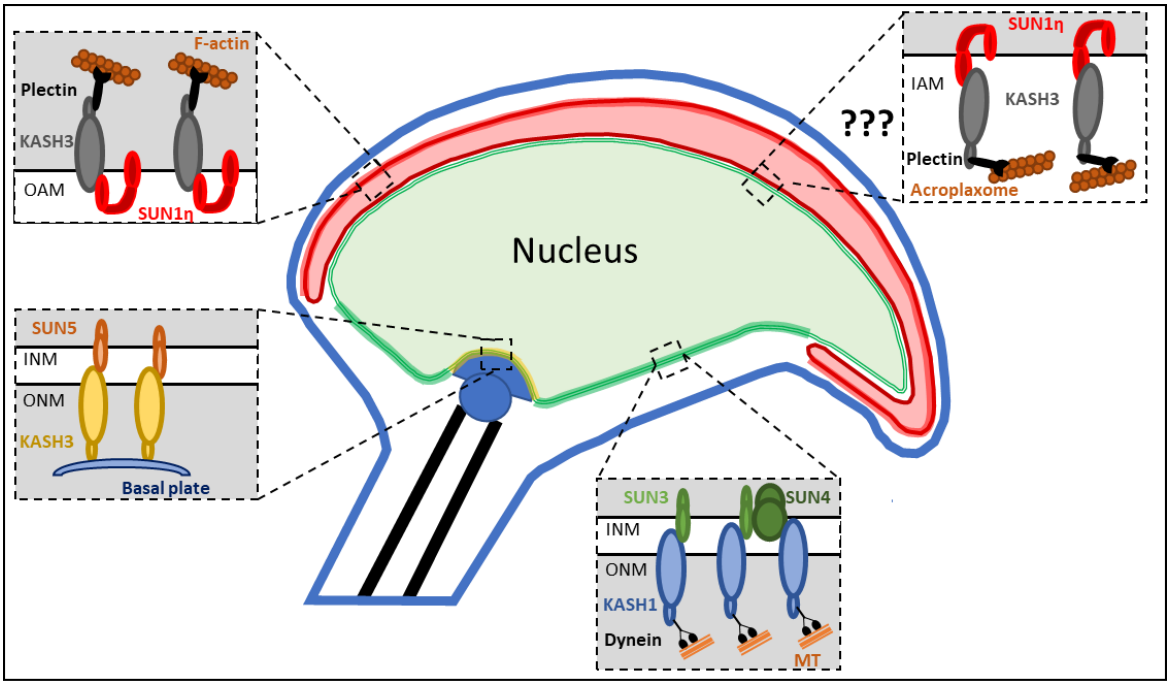

Figure 3: Graphical model illustrating LINC complex localization in maturated mouse sperm. Knowledge know about the sperm LINC complex so far is summarised in this figure. SUN5: KASH1 directly complex connects the head to tail and is exclusively located in the implementation fossa where it interacts with the basal plate. SUN3: SUN4: KASH1 complex is situated in the sub acrosomal region but is excluded from the implementation fossa. SUN1η: KASH1 complex in the OAM. Question marks represent hypothetical SUN1η: KASH1 located in the IAM with reversed orientation. The presence of this LINC complex was not documented so far. This illustration is inspired by the scheme in Göb et al., 2010.

spermatocytes to mature sperm. During meiotic division, SUN5 transiently forms a complex with KASH2 which is essential for the proper connection of telomers to the microtubules (Horn *et al*., 2013, Link *et al*., 2014).

2.2 Role of Lamin proteins in the nuclear lamina

The nuclear lamina is a complex network composed of lamin proteins and lamin binding proteins located just beneath the NE. Nuclear lamina plays many roles in various cellular processes. It is involved in nuclear positioning, chromatin reorganization, regulation of DNA replication and transcription, mechanotransduction (as it directly interacts with LINC), or regulation of mitosis and meiosis. (Paci *et al*., 2018, Pereira *et al*., 2019) In males, nuclear lamina is essential for the initiation of histone – protamine transition description of protamines in chapter 2.3). Protamine 1 binds to the Lamin B receptor (LBR) before its interaction with chromatin (Mylonis *et al*., 2004).

Lamins are type V intermediate filaments with complex structure. On the N-terminal end, a short non-helical globular head domain is located, connected to a long central α-helical rod domain. The C-terminal end contains nuclear localization signal, Ig-like domain, and CaaX motif (Fig. 4). Thanks to this structure, lamins are able to interact with each other in head-to-tail order (Pereira *et al*., 2019). CaaX motif can be isoprenylated, which is essential for targeting the lamin to the nuclear periphery but also enables the head of another lamin to bind there (Firmbach-Kraft and Stick, 1995).

There are three major types of lamins in mammals, encoded by three genes - *LmnA, LmnB1 and LmnB2*. Gene *LmnA* has the following splicing variants: A, AΔ10, C, and C2 (Gruenbaum *et al*., 2003). Generally, lamins A can be found in differentiated cells with one exception. Lamin C2 is a male meiosis-specific protein located in spermatocytes (Alsheimer and Benavente, 1996). Its main role is to maintain the attachment of telomeres to the NE during meiosis (Link *et al*., 2013). On the other hand, *LmnB1* is broadly expressed and can be found in both, differentiated and undifferentiated cells, including embryonic cells. *LmnB2* encodes two proteins - Lamin B2 and Lamin B3. All three Lamins B can be found in testes where they have different functions.

Changes in lamins expression can lead to several pathologies, generally known as laminopathy. During mechanical stress not only cytoskeleton is important for cell response but also lamins and NE play a crucial role. Therefore, laminopathies are in general connected with skin diseases, muscular dystrophy, cardiomyopathy neuropathy, Hutchinson-Gilford progeria, and many other diseases (Houben *et al*., 2007, Paci *et al*., 2018). Moreover, lamins can be crucial for proper embryonic development. Mice with mutated *LmnB1* died shortly after birth and had abnormally developed lungs and reduced long bone ossification (Vergnes *et al*., 2004).

Lamins and their biding proteins have an impact on fertility. For example, about 70 % of globozoospermia (a condition when a man has round-headed spermatozoa without acrosomes, and abnormal nuclear membrane) is caused by a mutation in *DPY19L2*. DPY19L2 is a LINC-like protein that interacts with LaminB1 and is essential for sperm head formation and acrosome development during spermiogenesis (Paci *et al*., 2018, Coutton *et al*., 2015). Mouse line with siRNA knockdown of *LmnA* gene exhibit acrosome malformation and disrupted acrosome integrity as proacrosomal vesicle docking in early steps of spermiogenesis is impaired (Shen *et al*., 2014). Other factors interacting with nuclear lamina are SUN proteins. It was shown in both, mice and humans, that any aberration in these genes causes a reduced or complete loss of fertility. Knockout mouse models for *Sun1*, *Sun3*, *Sun4,* and *Sun5* are completely sterile with abnormal sperm phenotypes (Kmonickova *et al*., 2020). In humans, 8 out of 17 infertile men with acephalic sperm had a mutation in *SUN5*. On the other hand, none of the mutations found were not present in healthy men (100 samples) (Zhu *et al*., 2016).

In the practical part of this work, Lamin B2 and Lamin B2/3 were studied. Therefore, Lamin A/C will be omitted from the theoretical part. Moreover, Lamins A/C are not involved in the process of spermiogenesis.

2.2.1 Lamin B protein family

Lamin B1 is ubiquitously expressed in all types of cells. It is encoded in humans by the *LMNB1* gene, in the mouse by the *LmnB1* gene. LmnB1 has been found in all stages of spermatogenesis. Its function is to decrease the mechanical strength of NE during meiotic chromosomes movements, enable dynamic sperm reshaping and head development and it also directs the chromatin distribution during spermiogenesis (Pereira *et al*., 2019). Interestingly, LmnB1 is the only Lamin to be found in human ejaculated spermatozoa. LmnB1 localization has been found by immunofluorescent microscopy on 33 % - 47 % of fresh human sperm. In addition, the percentage of Lamin B1 positive cells was significantly decreased in sperm selected by swim-

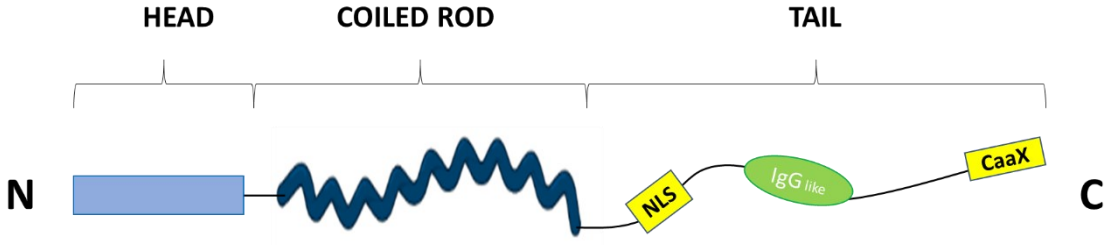

Figure 4: Schematic drawing of generic lamin structure. N-terminal head domain is flanked by coiled coil domain followed by tail with CaaX motif at the C-terminal end.

up or dense gradient centrifugation. These observations suggest that LmnB1 can have a link to the proper completion of sperm head compaction and thus act as a marker of sperm quality (Elkhatib *et al*., 2014). In mouse sperm, localization of LmnB1 was not reported yet.

Lamins B are located not only in the nuclear periphery but also in the nucleoplasm. Moir *et al*., 1994 showed, that B-type lamins can be found in the nucleoplasm where they colocalize with DNA replication sites during the S phase. Next, Lamin B2, encoded by the *LMNB2* gene, was found to be localized in the granular component of the nucleolus, where it interacts with nucleolar proteins – nucleolin and nucleophosmin. The head domain of LmnB2 has an essential role in the formation and modulation of dynamics of the nucleolus, the site where ribosome biogenesis starts (Sen Gupta and Sengupta 2017). Any aberration in ribosomal biosynthesis can lead to ribosomal stress, which is usually connected with impaired gnome integrity. Both, ribosomal biogenesis and genome integrity are essential for well-being and any discrepancy can result in various negative effects on the whole organism (Šanovec, 2019). So far, there was no proper evidence, that LmnB2 is involved in spermiogenesis (Vester *et al*., 1993). However, (Elkhatib *et al*., 2014) showed, that LmnB2 is expressed in a small amount in human testes. Their data from qPCR and immunohistochemistry suggests, that LmnB2 is present in human testicular cells but not in human spermatozoa.

On the other hand, Lamin B3 is described as a spermatogenesis-specific Lamin. LmnB3 is a shorter splicing variant of Lamin B2, both are encoded by the same gene. Its molecular weight is 53 kDa compared to Lamin B2 with 68 kDa. In mice, LaminB3 lacks 225 amino acids from the N-terminal end, therefore it is not able to form head-to-tail polymers. The N-terminal domain is replaced by a unique nonhelical 84 amino acid sequence. This feature makes LaminB3 the only Lamin which has a longer head domain than the central coiled-coil rod domain (Furukawa and Hotta 1993). Lamin B3 was detected in the male postmeiotic stages of spermiogenesis at the nuclear periphery but also in the nuclear interior. With the progression of spermiogenesis, it becomes polarized to the posterior, which suggests its colocalization with the implementation fossa (Schütz *et al*., 2005a). After ectopic expression in somatic cells the morphology of the nucleus changes to hook-like (Furukawa and Hotta 1993, Schütz *et al*., 2005b, Elkhatib *et al*., 2014). Therefore, it is suggested that Lamin B3 is essential for nuclear reshaping during spermiogenesis as it makes the nuclear envelope less stable and more flexible. These days there is no commercially viable antibody to study Lamin B3. Therefore, no data about Lamin B3 (trans)location and interactions in histological samples can be provided.

2.3 Role of Protamines in Sperm

Protamines are small proteins with high arginine content and the capability of binding to the DNA. They replace histones during spermiogenesis to ensure hypercondensation of chromatin by binding to the minor groove of the DNA. Protamine-DNA connection is stabilized by intra- and intermolecular disulfide bonds from cysteine residues resulting in about 6-fold denser DNA compaction than histones of mitotic chromosomes (Coelingh *et al*., 1969, Balhorn 1982, Ward and Coffey 1991), This hypercondensation is essential for maintaining sperm genome integrity via transcription silencing (Steger, 1999) and enables sperm to reduce its size. Therefore, sperm with condensed nuclei have better hydrodynamicity. (Woop *et al*., 2015)

There exist two types of protamines, protamine 1 (Prm1) and protamine 2 (Prm2). While Prm1 is present in all mammals, levels of Prm2 are variable in different species (Ammer *et al*., 1986). For example, in humans ratio of both protamines is about the same whereas in mice Prm2 is more abundant (65 % of total protamine level) (Corzett *et al*., 2002). On the other hand, some mammals such as bulls or boars, do not express Prm2, which is absent due to the mutation in the promoter region (Maier *et al*., 1990), and DNA packaging is organised by Prm1 protein only. The protamine ratio is important for sperm fertilizing ability. It was shown that the ratio of sperm Prm1 to Prm2 mRNA can be used as a clinical parameter to estimate men's fertility and fertilizing capacity for IVF or ICSI (intracytoplasmic sperm injection) (Rogenhofer *et al.*, 2013).

Histone to protamine exchange represents a crucial phase of spermiogenesis. It begins in elongating spermatids and the DNA hyper condensation is finished during the epididymal maturation. However, not all histones are replaced by protamines, and their amount is species-specific, e.g., 85 % of histones are replaced in humans compared to 99 % of histones replaced in mice (Gatewood *et al*., 1987, Brunner *et al*., 2014). The histone–protamine exchange is not random, more like it is a tightly controlled process. It was found that DNA from the centromeric region is not interacting with protamines nor with histones. However, Alu sequences, as well as telomeric regions, are fully bound to the protamines. (Wykes and Krawetz 2003).

2.3.1 Effect of *Prm2* deletion on mouse fertility

It is believed, that positively charged arginine groups of Prm2 neutralize negatively charged phosphate groups of the DNA. Therefore, the different 3D structure of the DNA-Protamine-

Histone complex in *Prm2*$^{-/-}$ mouse might influence the phenotype and properties of its sperm. (Cho *et al*., 2003)

In this thesis, the mouse line C57BL/6J Prm2Δ^{97}previously generated by Schneider and his colleagues in 2016 using the CRISPR Cas 9 system was used. Offsprings of this mouse line have deleted 97 bp in exon 1 which results in disrupted Prm2 gene functions. So far, two publications describing *Prm2*$^{-/-}$ mouse phenotypes have been published (Schneider *et al*., 2016, Schneider *et al*., 2020)

In general, loss of both *Prm2* alleles leads to infertility and affects only males. Females are not affected by the heterozygous or homozygous deletion. Secondly, in males, loss of one *Prm2* allele, seem to be compensated as *Prm2* heterozygous males resemble wild-type mouse in all studied parameters. *Prm2* full deletion affects not only DNA integrity in the sperm head but also the bending of the flagellum and anchorage of the acrosome. Testis weight, epididymal cell count, and testis morphology is not changed compared to wild type, which indicates that spermatogenesis might not be changed. Key phenotype changes of *Prm2*$^{-/-}$ mouse are listed below:

1. *Prm2*$^{-/-}$ sperm are completely immotile. Moreover, they do not react to exogenous calcium stimuli. Observations from the electron microscope suggest that the plasma membrane is damaged.
2. Midpiece of the flagellum of the *Prm2*$^{-/-}$ mouse is wrapped around the sperm head and the acrosome is detached.
3. On the ultrastructural level, *Prm2*$^{-/-}$ sperm display detachment of the acrosome at the acrosome-nuclear interface, which results in an abnormally shaped head with an undulating plasma membrane.
4. Nuclear matrix is impaired and abnormalities in chromatin condensation occurs from step 12 of spermiogenesis. These changes can be detected by electron microscopy.
5. Whereas *Prm2*$^{-/-}$ mice have severely disturbed chromatin integrity, degraded and damaged DNA in more than 80 % of cells, the heterozygous mouse keeps DNA unimpaired (over 90 % of *Prm2*$^{+/-}$ sperm is intact). Nevertheless, it is more than in the *Prm2*$^{+/+}$.
6. *Prm2*$^{-/-}$ sperm have reduced antioxidant capacity and are susceptible to reactive oxygen species (ROS) during epididymal maturation. ROS contribute to DNA damage and are responsible for membrane integrity disruption.

7. Epididymal sperm of *Prm2*$^{-/-}$ are fully immotile and lack the capability to fertilize an egg. This phenotype can be bypassed by ICSI of testicular sperm. Early embryo development was normal and comparable with early embryonic development where *Prm2*$^{+/+}$ sperm was used.

2.4 Septin 12

Septins are the fourth type of the cytoskeleton. These proteins have a conserved GTP binding domain and form a filamentous structure (Mostowy and Cossart, 2012). Septin 12 is expressed only in male postmeiotic cells (Lin *et al*., 2009). It is located in the manchette of elongating spermatids, in the neck of elongated spermatids and in the annulus (connection of the midpiece with the principal piece) of the maturated spermatozoa. In humans, point mutations in the *SEPT12* GTP-binding region were linked to teratozoospermia (morphologically abnormal sperm) and oligozoospermia (number of sperm is less than 15 million per milliliter of ejaculate). Moreover, Sept12 filamentous structure was disrupted. (Ihara *et al*., 2005, Lin *et al*., 2011). In the mouse knock-out model, it was shown, that *Sept12*$^{-/-}$ has a similar phenotype as *Sun4*$^{-/-}$. Both models have unphysiologically shaped sperm heads and aberrantly formed tails.

Later It was found that Sept12 is able to interact with SUN4 and LaminB as well as with Protamine2 (Yeh *et al*., 2015). SEPT12 forms the SEPT12/LmnB1/SUN4 complex where it forms a connection of SUN4 with the nuclear lamina. This complex is also important for the nuclear envelope stability. It was shown that mutation in the SPET12 reduces its ability to form the LmnB1/SUN4 complex. Cotransfection studies showed, that Septin 12 influences and directs the localization of LamninB1 and SUN4 (Yeh *et al*., 2019). As SUN proteins lead the localization of KASH proteins, any heavy defect in SEPT12 may result in miscommunication between the nucleus and the cytoskeleton by disrupting the LINC complex.

It was also found that SEPT12 can interact with α- and β- tubulin and has a role in head and tail development. The study made on mouse *Sept12*$^{+/+/+/-}$ chimeras showed unphysiologically formed heads with scattered α- and β-tubulin patterns. The sperm of this chimeric mouse also had bent and disorganised tails with disorganised α- and β-tubulin around the mid-piece, neck, annulus, and principal piece (Kuo *et al*., 2013)

2.5 Biogenesis and function of the acrosome

The acrosome is a specialized vesicular structure developed from the Golgi apparatus during spermiogenesis. Acrosomes, as well as matured spermatozoa, have different size and shape among different species. When sperm gets to a close proximity of an oocyte and its extracellular surroundings, these two membranes fuse during the process called the Acrosomal Reaction (AR). The AR is crucial for sperm to pass through the extracellular envelope in order to fuse with the oocyte plasma membrane (oolemma). During the AR, the proteolytic and hydrolytic enzymes located in the acrosome are released. One of the main enzymes released from the acrosome is hyaluronidase, which digests the zona pellucida, the outer glycoprotein layer of the oocyte (Larson and Miller, 1999, Yanagimachi, 2011).

Acrosome development was characterized in 1955. In mice, acrosome development consists of 16 steps, based on acrosome reshaping. These steps are divided into 4 phases: Golgi phase, Cap phase, Acrosome phase and Maturation phase (Burgos and Fawcett 1955, Khawar *et al*., 2019). Although the acrosome and its content are made by the Golgi apparatus and endoplasmic reticulum, there are other essential factors for proper sperm maturation (Khawar *et al*., 2019). One example can be the cytoskeleton. Trafficking of proacrosomal vesicles is mediated by microtubule network and tubulin-specific motors kinesins. It was shown that Kinesin-14 KIFC1 together with myosin Va, the molecular motor of F-actin, are present in Step1 and Step3-Step5 spermatids, respectively, and they colocalize with Golgi apparatus. Moreover, reduced KIFC1 expression was shown to be connected with a defective acrosome formation. (Yang and Sperry, 2003, Kierszenbaum *et al*., 2004, Zhi *et al*., 2016).

The next essential cytoskeletal structure during acrosome biogenesis is the acroplaxome. Term acroplaxome comes from three Greek words (akros = topmost; platys = flat; sõma = body). In sperm, the acroplaxome is a cytoskeletal structure located in the subacrosomal region made from F-actin and Keratin-5 (Kierszenbaum *et al*., 2003). This structure is essential for the proper connection of acrosome to the nucleus. Moreover, some studies suggest, that the acroplaxome can speed up the vesicular transport mediated by myosin-Va (Kierszenbaum *et al*., 2004, Dunleavy *et al*., 2019). The position of the acroplaxome is probably directed by some LINC complex and the ability of keratin-5 to bind to the nuclear lamina (Dunleavy *et al*., 2019).

Even though mammalian freshly ejaculated sperm are morphologically fully developed, they lack the ability to fertilize the egg. Sperm need to undergo maturation in the female reproductive tract, which final stage is called capacitation which can be defined by certain molecular changes

(Plant and Zeleznik, 2015). The plasma membrane obtains fluidity by the cholesterol efflux and its binding to the albumin and becomes permeable for ion exchange (Visconti *et al*., 1999a, Visconti *et al*., 1999b). Further, specific proteins are phosphorylated, mainly on tyrosine residues, by a signalling cascade mediated via protein kinase A (PKA). The phosphorylation events result in the influx of Ca^{2+} and cyclic adenosine monophosphate (cAMP). These two events lead to the crucial alteration in sperm motility. The sperm become hyperactivated, move faster with change in movement amplitude and the pattern of flagellum beating becomes asymmetrical (Ickowicz *et al*., 2012). However, sperm hyperactivation is essential for fertilization, it is not the only key event that happens in order to achieve successful oocyte-sperm fusion. Cytoskeleton, namely actin, must undergo certain changes such as polymerization followed by rapid depolymerization prior to the AR. This event is orchestrated by phosphatidylinositol 3 kinase (PI3K) and by actin-binding proteins such as testis-specific actin capping protein, gelsolin, Arp-T1, Arp-T2, calicin, destrin and many other proteins (Breitbart *et al*., 2005, Ickowicz *et al*., 2012)

The importance of actin polymerization during capacitation and its depolymerization during AR has been proven by many experiments on various species. When blocking the actin polymerization, for example by cytochalasin D, sperm is not able to fertilize the egg. Same results were observed, when actin depolymerization was blocked, resulting in no acrosomal reaction after its stimulation by zona pellucida (Brener *et al*., 2003, Breitbart *et al*., 2005).

2.6 Sperm motility

Sperm motility was defined as the propagation of transverse waves along the flagellum in a proximal-to-distal direction which results in a production of hydrodynamic impulse that pushes the sperm through the female genital tract to penetrate the oocyte (Paoli *et al*., 2011). In other words, sperm motility is an ability of sperm to move through the environment using a tail beating. At the end of the spermiogenesis, sperm cells are fully morphologically developed but immotile and gain the primary motility through the process of epididymal maturation (Freitas *et al*., 2017). Without the epidydimal maturation, sperm would be unable to fertilize the egg (Cornwall *et al*., 2009). The condition, when a man has reduced sperm motility is called asthenozoospermia. Specifically, asthenozoospermia is defined as less than 40 % sperm motility or less than 32 % with progressive motility. 100 % asthenozoospermia occurs at the frequency of 1 in 5 000 men. (Castañeda *et al*., 2018).

Sperm motility is tightly connected to the structure of the tail. The midpiece contains mitochondria which produce the energy needed for the motility. The principle and the end piece are responsible for generating the flagellar waveform pattern (Freitas *et al*., 2017). The core part of the tail is composed of the axoneme, a structure made from a central doublet of microtubules surrounded by 9 doublets. These microtubule doublets are connected to each other and to the central doublet via nexins. The waveform motility pattern is generated by sliding of tubulin doublets forced by kinesins. This mechanism is based on an "on-and-off" switch – while kinesins on the left side are active the kinesins on the right side are inactive and vice versa (Inaba, 2003, Lindemann and, Lesich, 2010, Freitas *et al*., 2017).

Recently, tubulin acetylation was shown to have an effect on sperm motility, particularly acetylation of α-tubulin at lysine 40 (α-tubulin acK40). This acetylation is known to be orchestrated by the coordination of αTAT1 (tubulin acetyltransferase 1) and HDAC6 (histone deacetylase) (Hubbert *et al*., 2002, Shida *et al*., 2010). A recent study revealed a decreased abundance of α-tubulin acK40 in asthenozoospermic men (Bhagwat *et al*., 2014). During the follow-up study, the same group discovered, that HDCA6 might act as a MAP, microtubule-associated protein and can modulate the rigidity or flexibility of the sperm axoneme. They also show showed that the abundance of α-tubulin acK40, HDAC6 and stabilizer of axonemal protein (SAXO1) is decreased in asthenozoospermic men (Chawan *et al*., 2020). It is important to note that these two studies used a different biological model than this thesis and tubulin acetylation patterns are species specific. For example, in two commonly used rodent model

organisms, the patterns are completely opposite. In rats, α-tubulin is acetylated in the whole length of the tail. On the other hand, the mouse tail has acetylated lysine only in the midpiece and endpiece (Ritagliati *et al*., 2018).

3 Hypothesis and Aims

This diploma thesis is part of the GACR and DGF bilateral grant on which the Laboratory of Reproductive Biology (IBT CAS) collaborates with the Laboratory of Molecular Andrology (JLU Giessen, Germany, Prof. Klaus Steger).

Hypothesis:

The LINC complex, which is located within the sperm nuclear envelope and connects the chromatin-cytoplasmic network system, represents the link between the loss of motility and the absence of protamine 2 in mouse *Prm2*$^{-/-}$ sperm. Analysis of the chromatin-cytoplasmic network system will provide a deeper into the functional connection between sperm chromatin remodeling and transmission of cytoplasmic driving forces to the flagellum.

Aims:

1. To characterize spermatid and sperm-specific localization of nuclear and cytoplasmic proteins of LINC complex in wild-type (WT) and Prm2$^{-/-}$ mice and identify new binding partners.
2. To compare protein and mRNA profiles of candidate proteins in testes, epididymis and sperm in WT and Prm2$^{-/-}$ mice.

4 Material

4.1 Animals

Protamine2 knock-out mouse (*Prm2*$^{-/-}$) line was prepared in Bonn by Schneider and his colleagues in 2016. Using Crispr/Cas 9 system, 97 bp deletion was introduced into *Prm2* exon 1 between 120-217 bp. This modification results in a frameshift that induces premature stop codons occurrence and nonsense transcript production. This mouse line was registered as C57BL/6J Prm2Δ^{97}. Wild-type (WT), *Prm2*$^{+/+}$, C57BL/6J males served as a control. Mice were housed in a breeding colony of the Laboratory of Reproduction, IMG animal facilities, Institute of Molecular Genetics of Czech Academy of Science, and food and water were supplied ad libitum. The male mice used for all experiments were healthy, 10–12 weeks old, with no sign of stress or discomfort. All animal procedures and experimental protocols were approved by the Animal Welfare Committee of the Czech Academy of Sciences, Animal Ethics protocol code 66866/2015-MZE-17214, 18 December 2015.

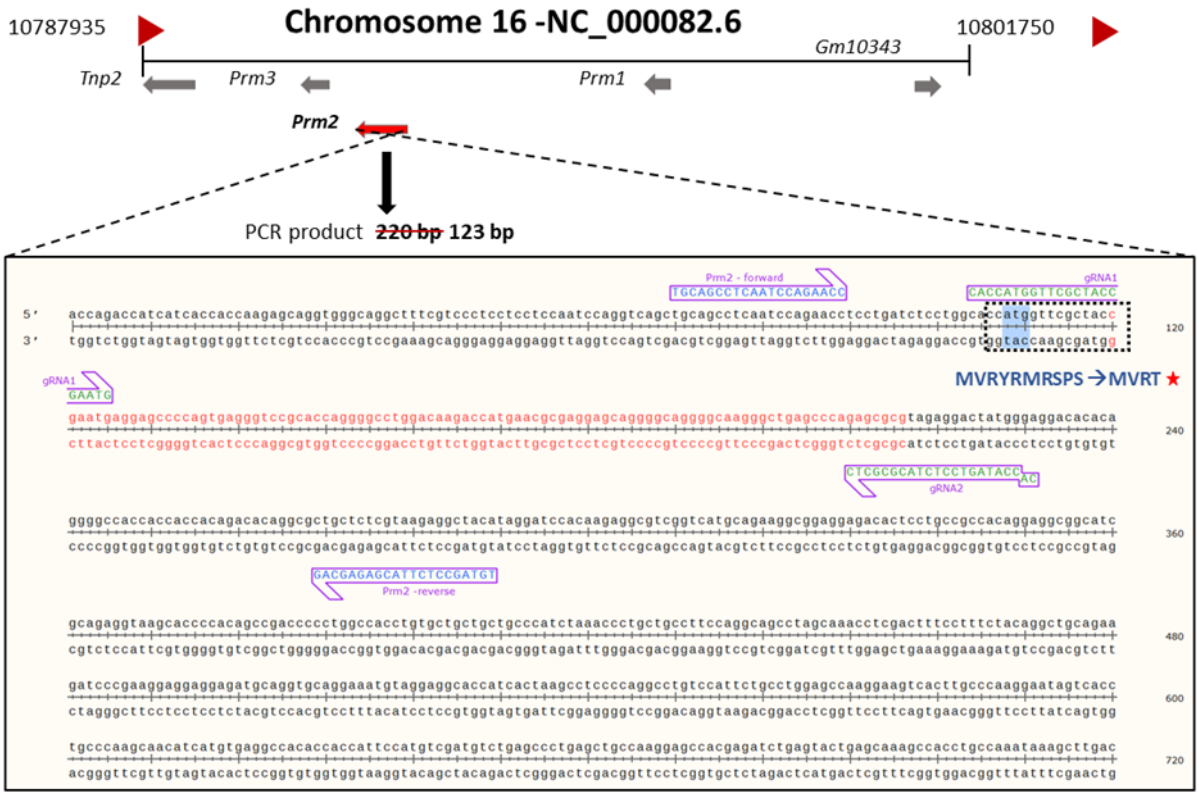

Figure 5: Graphical illustration showing deletion in mouse exon 1 of *Prm2* gene. Blue highlight shows start codon. Deletion between 120 – 217 bp is shown in red. Asterisk represents stop codon. *Prm2* allele was analysed by Sanger sequencing. Primers for genotyping are in blue, guide RNAs for Crispr/Cas 9 are shown in green. Primers were designed by Schneider *et al.*, 2016.

4.2 Buffers and solutions

2 % agarose	1,6 g of agarose in 60 ml of TAE buffer, 2 µl of Gel Red
50x TAE	242 g of Tris, 18,61 g of disodium EDTA, 57,1 ml of acetic acid were dissolved in ddH_2O to a final volume of 1 l
Buffered formalin	10 % formaldehyde in PBS, pH 7,4
CBB staining	0,25 g of CBB, 35 ml of acetic acid, 250 ml of ethanol, 215 ml of dH_2O
Citric buffer pH 6	11,5 ml of solution A (2,1 g of citric acid in 100 ml of dH_2O) mixed with 88,5 ml of solution B (2,9 g of sodium citrate dihydrate in 100 ml dH_2O). Adjust pH to 6
Electrode buffer	10x 60,6 g of Tris, 288g of glycine, 20 g of SDS dissolved in 2 000 ml of dH_2O
Gel monomer	2 ml of Acrylamide 40 %, 0,5 ml of Bis-Acrylamide 20 %, 0,5 ml of 10% VA-044 initiator, 2 ml of 10x PBS, 5 ml of 16 % methanol free formaldehyde, and filled with water to 20 ml
PBS	87,7 g of NaCl and 27,6 g of $NaH_2PO_4x2H_2O$ were dissolved in 1 l creating 10x concentrated PBS. To make 1x PBS 100 ml of 10x PBS were diluted to 1 l of dH_2O and pH was adjusted to 7,4
SDS clearing buffer	1,68 g of LiOH x H_2O and 115,35 g of SDS dissolved in 2 000 ml of H_2O. pH adjusted to 8,5 by H_3BO_3
SDS lysis buffer	1 ml of 0,5M Tris-HCl pH8 buffer, 0,8 ml of glycerol and 1,6 g of SDS dissolved in 4,2 ml of H_2O 242 f of Tris, 18,61 g of disodium EDTA, 57,1 ml of acetic acid were dissolved in ddH_2O to a final volume of 1 l

4.3 Consumables

15 / 50 ml Tubes	TPP
Cover slides	Hirschmann
Glass slides	Marienfeld
Imaging chambers	Grace Bio-Labs
Microtubes	Eppendorf
Nail polis	Common drug store
Pipet tips	Eppendorf
Super frost microscopy slides	Thermo Fisher Scientific

4.4 Chemicals

2-Mercaptoethanol	Sigma-Aldrich
Acetic acid	Penta
Acrylamide	Bio-Rad
Agarose	Carl Roth
Antibody diluent	Zytomed Systems GmbH, ZUC025-100
APS	Sigma-Aldrich
Boric acid	Sigma-Aldrich
Brom phenol blue	Sigma-Aldrich
CBB	Serva
Citric acid	Biorad
DAPI	Vector Laboratories
Diasolve	DiaPath
DMSO	Sigma
DNase I buffer	Thermo Fisher Scientific
DNase I	Thermo Fisher Scientific
dNTPs	Thermo Fisher Scientific
EDTA	Thermo Fisher Scientific
Ethanol	Penta
Formaldehyde methanol-free	Thermo Fisher Scientific
Formalin buffered	Sigma
Gel red	Botium
Glycerol	Sigma-Aldrich
Glycine	Serva
Kit for mRNA isolation	Qiagen
Lithium hydroxide	Sigma-Aldrich
M2 medium	Sigma-Aldrich
Ponceau’s	Sigma-Aldrich
Precision Plus Dual Color	Bio-Rad

Random primers for RT	Thermo Fisher Scientific
Riboblock inhibitor	Thermo Fisher Scientific
RT reaction buffer	Thermo Fisher Scientific
SDS	Sigma-Aldrich
Skimmed milk	Santa Cruz Biotechnology
Sodium citrate dihydrate	Biorad
Spike RNA	TATAA box
Super Block	Thermo Fisher Scientific
Super signal West Substrate	Thermo Fisher Scientific
SYBR green	Bio-Rad
TEMED	Sigma-Aldrich
Tris	Serva
Triton	Serva
VA-044 initiator	Fujifilm
Vectashield Mounting Medium	Vector Laboratories
RNeasy Plus Mini Kit	Qiagen

4.5 Laboratory equipment

Azure 600 detection system	Azure
Centrifuge 5804 R	Eppendorf
Centrifuge Mini spin plus	Eppendorf
CO_2 incubator	Eppendorf
Confocal microscope	Carl Zeiss LSM 880 NLO
Cycler for PCR	Touchgene
Cycler for qPCR	Bio-Rad
Electrophoretic system	Bio-Rad
Microscope lightsheet	Zeiss Lightsheet Z.1
Microscope	Olympus IX81
Microtome	Leica
Nanodrop	Thermo Fisher Scientific

Orbital shaker PSU-10i	Biosan
Qubit fluorometer	Invitrogen
Set of pipets	Eppendorf
Spinning disc microscope	Nikon CSU-W1 spinning disc microscope
Stereomicroscope	Olympus
ThermoCell MixingBlock	Bioer
Tissue homogenization	Bertin
Turboblot system	Bio-Rad
Vortex mixer	P-Lab

4.6 Software

Biorender.com

GraphPad

Image J

IMARIS

MS Excel

MS PowerPoint

NIS-Elements

Zen blue

5 Methods

5.1 Mouse genotyping

Two weeks old mice underwent a tail biopsy and obtained tissue was used as material for mouse genotyping. At first, DNA was extracted by adding 180 µl of 50 mM NaOH. Samples were vortexed vigorously, shortly spined and incubated in the thermoblock with shaking for 10 minutes at 95 °C and 500 rpm. After that, 20 µl of 1M Tris, pH 8 were added to each sample followed by vortex and centrifugation for 10 minutes at 12 000 rpm.

Next, 19 µl PCR mix per sample was prepared. Mix was prepared by mixing 10,8 µl H_2O, 2 µ 10X LA PCR buffer, 2 µ 25 nM $MgCl_2$, 2 µ of 2,5 mM dNTP, 2 µ of 10 pmol primers (Forward + reversed premixed together), 0,2 µl of La Taq polymerase.

1 µl of isolated DNA was added to 19 µl of PCR mix and amplified on a cycler (Touchgene). PCR setting is shown in the following table. Primer sequences are shown in table 3.

Table 1: PCR protocol

Step	Temperature (°C)	Time	Number of cycles
Starting denaturation	94	60 seconds	1
Denaturation	94	30 seconds	30
Hybridization	60	30 seconds	30
Elongation	72	120 seconds	30

Amplified DNA was analysed on 2 % agarose gel mixed with gel red. Electrophoresis took 1 hour with the constant setting of 100 V. Results were visualized on Bio-Imaging Systems, MiniBIS Pro.

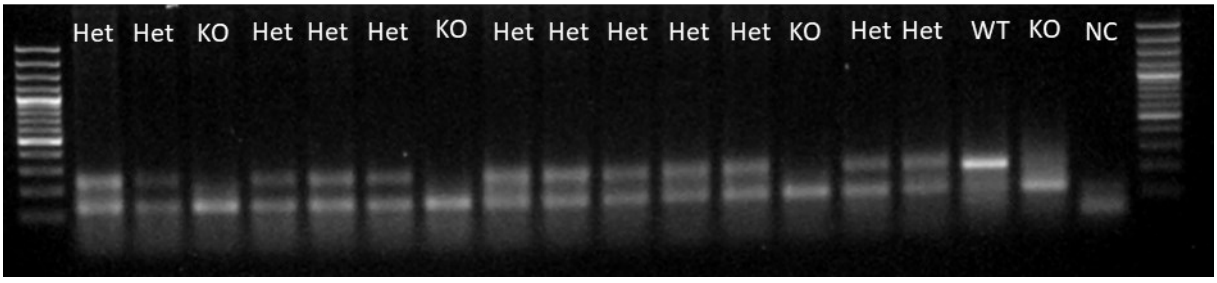

Figure 6: Representative example of results from PCR genotyping. Mouse genotype was analyzed on 2 % agarose gel. NC = negative control, Het = $Prm2^{+/-}$, KO = $Prm2^{-/-}$, WT = $Prm2^{+/+}$.

5.2 Sperm isolation and smear preparation

Sperm cells were obtained by the swim-up method. Mouse cauda epididymis was harvested and transferred into a 200 µl drop of M2 medium preheated to 37°C. The tissue was gently cut with scissors and incubated in the incubator at 37°C, 5 % CO_2 for 15 minutes. Medium with released sperm was transferred into an Eppendorf tube and centrifuged for 5 min at 300 g. Supernatant was removed and the pellet was gently resuspended in PBS and centrifuged again. The supernatant was removed, and the sperm pellet was ready to use. Sperm were used either for microscopy (chapter 5.4) or western blot (chapter 5.7).

The sperm pellet was resuspended in PBS. 5 µl of suspension was used to make 1 smear on a glass microscopy slide. Smears were air-dried, fixed in formalin for 15 minutes, washed in PBS for 5 minutes and then stained. Sperm were incubated in Superblock solution for 1 hour at RT. The following steps are identical to the staining of paraffin sections (see chapter 5.4).

5.3 RNA isolation, RT-PCR and qPCR

30 mg of testicular tissue was homogenized in Tissue homogenization (Bertin). RNA was isolated using RNeasy Plus Mini Kit according to the manufacturer's instructions. The concentration of isolated RNA was measured on NanoDrop (Thermofisher scientific)

Three-step reverse transcription PCR (RT-PCR) was done using the following protocol.

STEP 1	Samples were treated with DNase I for 30 minutes at 37°C. 1µg of RNA was mixed with 1 µl o Dnase I and 1 µl of Dnase buffer. The reaction was filled to 10 µl with water.
STEP 2	Dnase chelation was performed for 10 minutes at 65°C. 1 µl of EDTA was added to each sample.
STEP 3	Reverse transcription was performed for 1 hour at 42°C followed by 10 minute incubation at 70°C. Each sample was supplemented with 4 µl of 5x Reaction buffer, 0,5 µl of Riboblock inhibitor, 2 µl of Spike RNA, 2 µl of 10 mM dNTP mix, 1 µl of oligo(dT)18+Random primers and with 1 µl of reverse transcriptase.

Obtained cDNA was diluted 10x and used as a template for qPCR.

The reaction mixture was prepared using 5 µl of SYBR, 2 µl of H_2O and 1 µl of primer mix per sample. Then, 2 µl of diluted cDNA were added.

qPCR was performed on Bio-Rad CFX-96 cycler with the following setup (see table 2). Primer sequences are shown in table 3. All primers were designed in Primer Blast software and manufactured by Generi Biotech company.

Table 2: qPCR protocol

Step	Temperature (°C)	Time	Number of cycles
Starting denaturation	95	10 minutes	1
Denaturation	95	15 seconds	35
Hybridization	60	30 seconds	35
Elongation	75	30 seconds	35

Table 3: Primer sequences and their authors for mouse genes.

Gene	Primer sequence (5'→3')	Author
RPS2	CTGACTCCCGACCTCTGGAAA GAGCCTGGGTCCTCTGAACA	Eva Žatecká
SUN4	GAACCGTCTGGATCTTCTGTAGT AGTGAACAGGAAGCGGATGG	Ondřej Šanovec
SUN3	AGGGGCTATCACACAGTCCT TTCCAACGTCTGTCTCAGCC	Ondřej Šanovec
KASH1	TCTGACACACGGTGGGAAAAT CCGTGTTAGCCACAGGTGAT	Ondřej Šanovec
ODF1	GTGACCTCTACTACCCGTGC TCTTTCACGCGCACTTTGAC	Ondřej Šanovec
LmnB2	CTGGCACACTACATCGACCGT TCCCGCTTCTTGGCACTCTTC	Ondřej Šanovec
LmnB2/3	AGGCTGCAAAGCACTCATCT TTCACATCAGTCGGCAGCCC	Ondřej Šanovec
LmnB3	AGGACTTGGAACAACCACCTC GCCTTGTCATTCTGGTCCGA	Ondřej Šanovec
Prm2	TGCAGCCTCAATCCAGAACC TGTAGCCTCTTACGAGAGCAG	Schneider et al., 2016
ActB	CGGTTCCGATGCCCTGAGGCTCTT CGTCACACTTCATGATGGAATTGA	Eva Žatecká
TUB5A	AAACCGTAGCCATGAGGGAAATCG CGTGGTAGGTACCGGTGGGGT	Eva Žatecká
TUB5B	TCAGTAAACCGTAGCCATGAGGGAA CAGCTGCAGGTCGCTGTCACC	Eva Žatecká
Septin12	GGGGCATCATCGAAGTGGAA CATTGTGGGTGATGTCCTTCAG	Ondřej Šanovec

5.4 Immunohistology and confocal microscopy

Mouse testes were harvested and fixed in buffered formalin solution for 48 hours at 4°C. After the fixation, the organs were embedded into paraffin wax, sectioned on a microtome (Leica) on 5 µm thick sections and transferred on Super frost microscopy slides. Prior to antibody labelling, sections were deparaffinized and hydrated. Samples were treated 2x with DIASLOV for 5 minutes followed by rehydration in decreasing ethanol series (100 %, 90 %, 70 %, H_2O, PBS). Each step took 5 minutes.

After that, antigens were retrieved by boiling the samples for 15 minutes in citrate buffer, pH 6. After 15 minutes samples were let to cool down to room temperature (RT). To block unspecific epitopes, samples were treated with Super Block solution for 1 hour at RT. Next, primary antibodies diluted in Antibody diluent were applied. Incubation took place at 4°C overnight. The next day, samples were washed in PBS for 3 x 5 minutes. After that, secondary antibodies diluted in Antibody diluent 200x together with peanut agglutinin (PNA) diluted 500x were applied for 1 hour at RT in dark. Samples were washed again 3 x 5 minutes in PBS and stained with DAPI diluted 500x in PBS. The staining lasted 5 minutes and was followed by washing in PBS for 5 minutes and 1 minute in dH_2O. Antibody labelled samples were air-dried in the dark and mounted into a Vectashield medium.

Because not all antibodies were able to stain their corresponding protein, different approaches were applied. Using cryosections instead of paraffin sections gave no results for none of the antibodies and the tissue morphology was pure. Another step to be optimized was antigen retrieval. Instead of using a citrate buffer of pH 6, I tried to use Tris-EDTA pH9 buffer or omit the antigen retrieval step. None of these two approaches gave satisfactory results.

Table 4: List of primary antibodies, catalogue numbers and dilution used.

Protein	Host	Catalogue number	Dilution
Lamin B2	Rabbit	AB_2533107	100x
Lamin B2/3	Rabbit	ab151735	50x
SUN4	Mouse	sc-393115	50x
SUN3	Rabbit	orb 13213	50x
Acetylated Tubulin K40	Mouse	sigma T7451	50x
α tubulin	Mouse	A11126	50x
ODF1	Rabbit	PA569988	50x
KASH1	Mouse	orb640301	50x
β actin	Mouse	ab 6276	50x
Septin 12	Mouse	H00124404-B01P	50x

Table 5: List of secondary antibodies and other fluorophores, catalogue numbers and dilution used.

Description	Host	Catalogue number	Dilution
Alexa fluor 568 anti-rabbit	Donkey	A10042	300x
Alexa fluor 568 anti-mouse	Donkey	A10037	300x
Alexa fluor 488 anti-rabbit	Goat	A11008	300x
Alexa fluor 488 anti-mouse	Goat	A11029	300x
DAPI	-	D1306	500x
PNA AF488 / AF568	-	L21409 / L32458	500x

5.5 CLARITY of individual seminiferous tubules – protocol optimization

To study spermatogenetic processes in the broader picture, a new protocol for tissue preparation was optimized. The protocol is based on the CLARITY method published by (Chung *et a*l., 2013). This method was originally developed for imaging whole organs, in this case mouse brains.

At first, individual seminiferous tubules (STs) were isolated using a fine tweezer in a drop of PBS under the stereomicroscope. Next, STs were incubated in the gel monomer for 2 hours at 4°C. According to the original protocol, the next step is polymerization of the organ submerged and infused with monomer solution. For our, significantly smaller biological samples, the following conditions were optimized: Shape of the monomer solution drop (linear or drop-like,

see Fig. 17.A) surface and the environment (vacuum, CO_2 incubator, N_2 atmosphere). Regarding the surface for gel polymerization, two materials were tested: Glass microscopy slides and slides coated with parafilm. For a description of other experimental conditions see table 6. It is known that gel polymerization needs to take place at 37°C and inert atmosphere as oxygen inhibits the polymerization reaction. Therefore, the following conditions seem to be best for gel polymerization: Incubation on a glass slide for 7 minutes in the N_2 atmosphere on a heat block preheated to 37°C with linearly shaped gel monomer matrix.

Table 6: Table of experimental conditions for optimal gel monomer polymerization testing. X = gel is still liquid, - = was not measured.

Time (min)	The shape of gel monomer	CO_2 incubator	Vacuum	N_2 atmosphere
5	Drop	X	X	X
	Linear	X	X	Partially polymerized
10	Drop	X	X	X
	Linear	X	X	Partially dried out
15	Drop	X	X	X
	Linear	X	Polymerization starts	-
20	Drop	X	X	X
	Linear	X	Edges dried out, The middle part is partially polymerized	-
60	Drop	X	Polymerization starts	X
	Linear	X	The sample is dried out	-

Monomer solution polymerization is followed by sample clearing in SDS buffer at 37°C with gentle shaking. Clearing time was optimized as well. Samples were cleared for 1 – 5 days. Best results were obtained after clearing for 24 hours. The quality of samples which were cleared for a longer time was dramatically reduced. It seems that long clearing has a negative effect on epitopes and therefore antibodies could not label the sample properly.

Cleared samples were incubated in primary antibodies (dilution 1:100). Three different diluents were used: PBS, Antibody diluent and PBS + 10 % DMSO + 0,1 % Triton. Samples were incubated on an orbital shaker for 66 hours at RT with shaking at 100 RPM. After that, samples were washed 3 x 2 hours in PBS at RT with shaking. Next, samples were incubated in secondary antibodies, PNA and DAPI all diluted 1:500 PBS /Antibody diluent / PBS + 10 % DMSO + 0,1 % Triton. Incubation took 42 hours at RT with shaking at 100 RPM. Samples were covered in aluminium foil to prevent them from photobleaching. Samples were washed again 3 x 2 hours in PBS at RT with shaking. Stained samples were incubated in 80 % glycerol overnight at RT in the dark. The next day, samples were mounted into fresh 80 % glycerol in imaging chambers

(35 x 19 x 0,6 mm) and covered with cover glass. Edges were sealed with transparent nail polish.

Prepared samples were evaluated under the confocal microscope Carl Zeiss LSM 880 NLO or on Nikon CSU-W1 Spinning Disk. Obtained data were analysed in software ImageJ and IMARIS.

5.6 Sperm protein extractions

Sperm cells were obtained as described in chapter 5.2. The sperm pellet was mixed with SDS lysis buffer, vortexed and incubated on ice for 30 minutes. Every 5 minutes, cells were vortexed again. After the incubation, samples were centrifuged for 2 minutes at 4°C with 10 000 g. The obtained supernatant was transferred to a fresh Eppendorf tube and protein concentration was measured according to the manufacturer's instruction using the Qubit fluorometer kit from Invitrogen. Next, protein extract was mixed with gel loading buffer and with β-mercaptoethanol (5 % of the lysate volume).

5.7 Western blot

10 % Acrylamide gels were prepared using Mini-PROTEAN Tetra Cell Bio-Rad equipment.

Table 7: Composition of running gel (10 % acrylamide).

Component	Volume (ml)
H_2O	7,00
30 % Acrylamide mix	4,00
1,5 M Tris (pH 8,8)	3,80
10 % SDS	0,15
10 % APS	0,15
TEMED	0,009

Table 8: Composition of stacking gel (5 % acrylamide).

Component	Volume (ml)
H_2O	3,40
30 % Acrylamide mix	0,83
0,5 M Tris (pH 6,8)	0,63
10 % SDS	0,05
10 % APS	0,05
TEMED	0,005

After gel polymerization, a volume corresponding to 25 ng/ml of protein was loaded per well. 3 µl of Precision Plus Protein™ Dual Colour Standards were used as a reference ladder. Electrophoresis of protein samples was done in Bio-Rad equipment. The electrophoretic vessel was filled with a running buffer and a constant voltage of 80 V was applied for 20 minutes. After that, the voltage was increased to 140 V for 1 hour.

Western blot was done using equipment Trans-Blot Turbo transfer system from Bio-Rad with material provided by the manufacturer (blotting buffer, PVDF membrane, papers). Western blot was performed for 10 minutes with a constant current of 2,5A.

After protein transfer, the membrane was stained with Ponceau's to visualize proteins on the membrane. Using a sharp scalpel, the membrane was cut to pieces and washed 5x in distilled water to remove the Ponceau's staining. Next, membranes were incubated in blocking solution (5 % skimmed milk) followed by primary antibody staining. Antibodies were applied overnight at 4°C. Following antibodies were used. Antibodies were diluted into the blocking solution.

Table 9: List of primary antibodies for western blot.

Protein	Host	Catalog number	Dilution
Acetylated α-tubulin K40	Mouse	sigma T7451	1:600
α-tubulin	Mouse	A11126	1:600
β-actin	Mouse	ab 6276	1:600
β-tubulin	Rabbit	T8355	1:600

The next day, membranes labelled with primary antibodies were washed in PBS + 0,1 % Tween for 3 x 10 minutes at RT on an orbital shaker. Secondary antibodies conjugated with horseradish peroxidase (HRP) were applied for 1 hour at RT. Antibodies from Bio-Rad company against mouse or rabbit IgG were used. Secondary antibodies were diluted into the PBS 1:3 000. After the incubation, membranes were washed again in PBS + 0,1 % Tween for 3 x 10 minutes at RT on an orbital shaker. After that 0,5 ml of SuperSignal™ West Pico Chemiluminescent Substrate was applied to each membrane and visualization take place on the Azure 600 machine.

Membranes were then stained with Coomassie Brilliant Blue staining to visualize protein loading on the membrane. This served as a loading control and the relative protein amount was quantified according to this membrane using Image J.

6 Results

6.1 Cytoskeletal proteins are affected by *Prm2*$^{-/-}$ deletion on the gene expression level

To monitor hypothesised changes in LINC and its partners on the gene expression level, qPCR of mRNA isolated from adult mouse testes was performed. The following genes were analysed: *LaminB2*, *LaminB3*, *LaminB2/3*, *SUN3*, *SUN4* and *KAHS1*. None of these targets show a significant change in mRNA level in *Prm2*$^{-/-}$ mouse (Fig. 7) As a reference gene, *Rps2* was used. Relative gene expression (ΔCq values) was analysed by inference statistic using the Mann-Whitney test in GraphPad software.

Results from western blots (Fig. 11) indicated changes in β-actin in Prm2$^{-/-}$. Therefore, levels of mRNA of cytoskeletal genes (*Tub5A, Tub5B, ActB, Sept12*) in the mouse testes were analysed by qPCR. Relative mRNA levels were normalized using the *Rps2* gene as a reference.

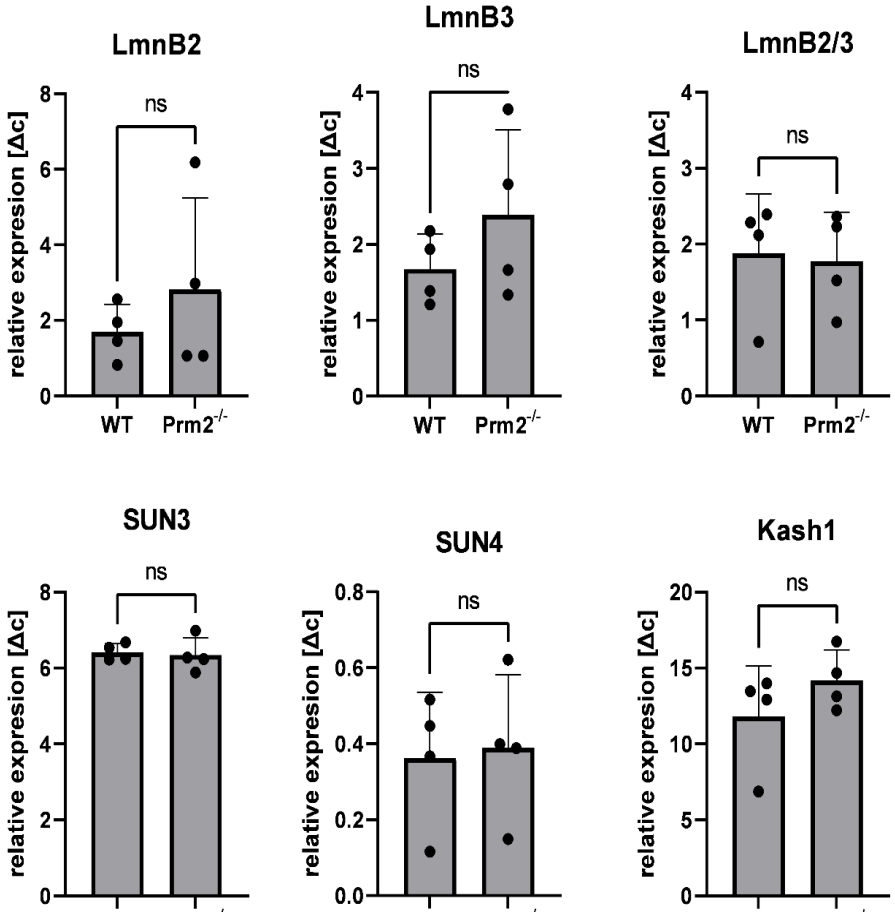

Figure 7: Comparison of relative gene expression of LaminsB and LINC-related proteins in WT and Prm2$^{-/-}$ *mouse testes. None of the measurements is significant. Analysed by Mann-Whitney test. n=4. Black dots represent the range of measured values. ns = not significant.*

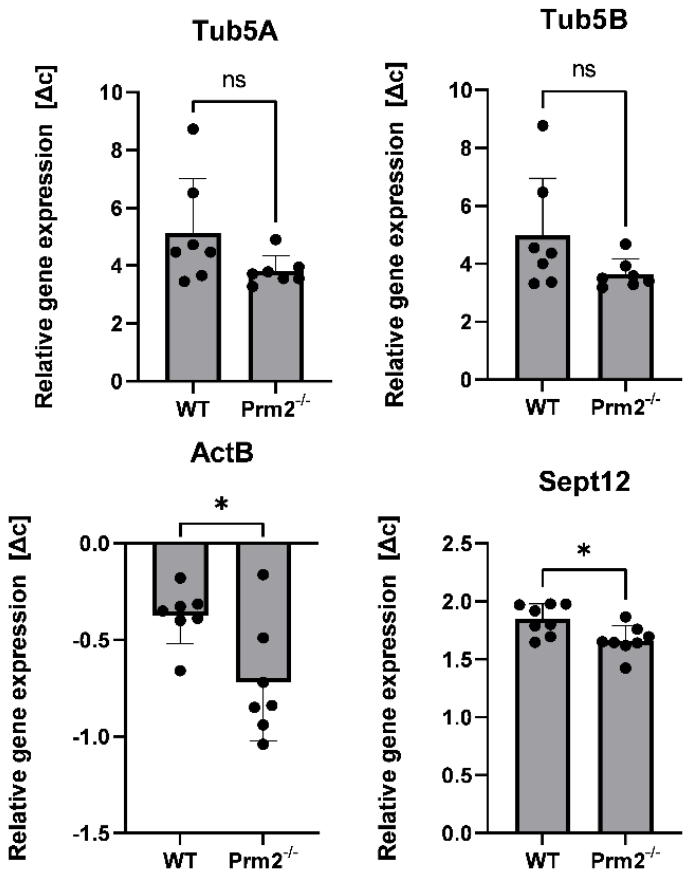

*Figure 8: Comparison of relative gene expression of cytoskeletal proteins in WT and Prm2$^{-/-}$ mouse testes. Analysed by Mann-Whitney test. n=7. Black dots represent the range of measured values. * represents p<0,05. ns = not significant.*

Gene expression of 7 individuals for each group was analysed and statistical analysis using the Mann-Whitney test showed decreased expression of β-actin and Septin 12 in Prm2$^{-/-}$ mouse testes compared to the wild type ($p < 0,05$) (Fig. 8).

6.2 Tubulin acetylation pattern is changed in *Prm2*$^{-/-}$ sperm

Next, the tubulin acetylation pattern was analyzed. Using sperm smears, confocal microscopy and immunofluorescence, the pattern of acetylation of α-tubulin at lysine 40 (α-tubulin acK40) was analyzed.

In WT mouse sperm, the α-tubulin acK40 signal was located mainly in the midpiece and end piece of the tail. However, in *Prm2*$^{-/-}$ mouse, tubulin seems to be acetylated in the whole tail. The fluorescence signal observed was homogeneously distributed through the whole Prm2$^{-/-}$ sperm tail (Fig 9.B).

Smeared sperm were stained for α-tubulin as well to check that sperm tail composition is not influenced by *Prm2*$^{-/-}$ deletion. As expected, the α-tubulin signal can be detected from the whole sperm tail in both, WT and *Prm2*$^{-/-}$ mouse sperm (Fig. 9.A).

To check if the tubulin acetylation is a product of epididymal maturation or happens already during spermiogenesis in the testes, paraffine testes sections were stained. The bright signal was observed in the lumen of seminiferous tubules with maturated spermatozoa showing localization of α-tubulin acK40 in the testicular sperm tails. The brighter signal was observed in the Prm2$^{-/-}$ testes, indicating, that tubulin acetylation probably happens already during spermiogenesis (Fig. 10).

The staining of testes against α-tubulin gave similar results in both, *Prm2*$^{-/-}$ and wild-type samples. α-tubulin was observed in the posterior part of the spermatid, in the regions where the signal for acrosome (PNA) was negative (Fig. 10).

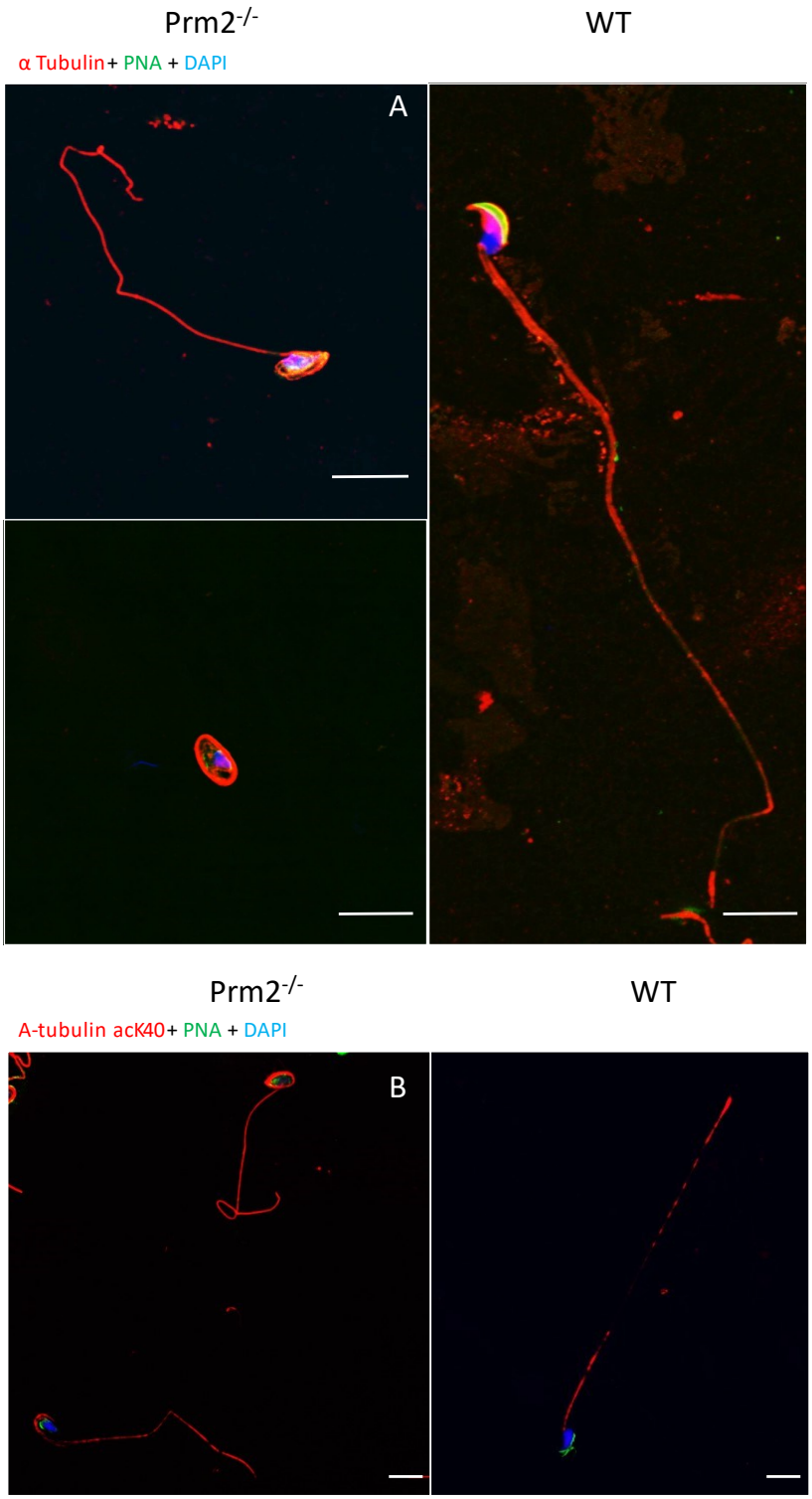

Figure 4: Representative picture of tubulin acetylation pattern in sperm tail. Acrosomes are shown in green; the nucleus is in blue. Scale bar = 10 µm.
A) *α-tubulin (in red) is distributed in the whole sperm tail in Prm2$^{-/-}$ as well as in WT.*
B) *α-tubulin acK40 (in red) is distributed in the whole sperm tale Prm2$^{-/-}$. α-tubulin acK40) is distributed mainly in the midpiece and principal piece of WT sperm.*

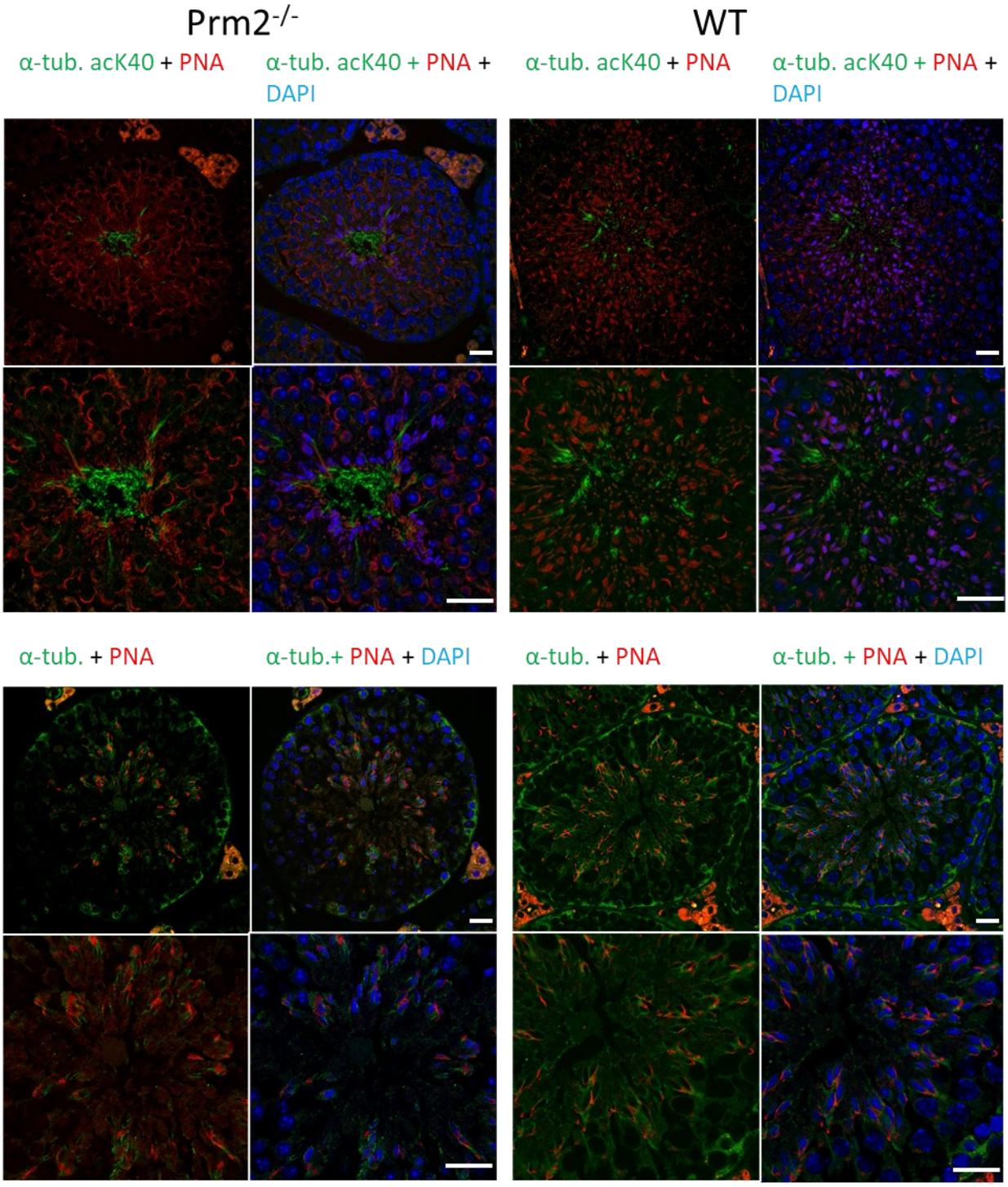

Figure 5: Representative examples showing localization of acetylated α-tubulin at lysine 40 and α-tubulin in Prm2$^{-/-}$ and WT testes. Paraffined testes sections, 5µm wide. Objective 63x, zoom 0,6 (top) and 1,2 (bottom). Scale bar = 20 µm

6.3 β-actin but no other cytoskeletal proteins abundance is changed in Prm2$^{-/-}$ sperm

Based on the observation of different patterns in tubulin acetylation, Western blots were performed to analyze the abundance of α-tubulin acK40. To be able to normalize and quantify protein amount, the β-actin was chosen as a loading control. Surprisingly, the amount of β-actin is significantly enriched in *Prm2*$^{-/-}$ sperm, compared to wild type ($p < 0{,}0001$). Therefore, a membrane stained by CBB was used for normalization and substituted a loading control protein. Other cytoskeletal proteins abundance (α-tubulin and β-tubulin) seems to be unaffected. Representative western blot results are shown in figure11. Whole membrane pictures can be found in the supplementary figure 1.

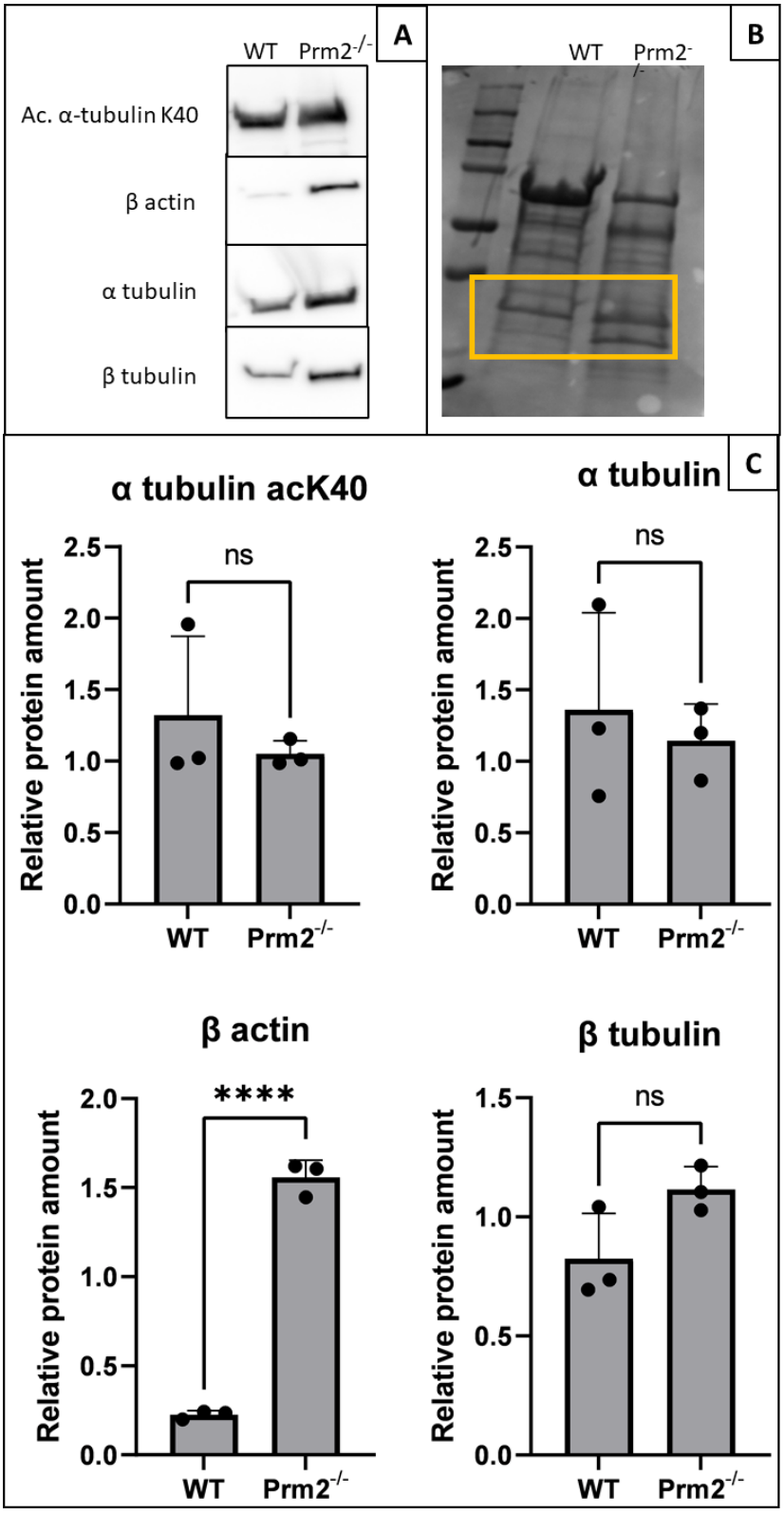

*Figure 6: **A)** Representative Western Blot showing band intensity for proteins of interest. In Wild type and Prm2-/- sperm lysates. **B)** Membrane stained with CBB. The yellow box shows the area used for quantification that served as a loading control. Whole membrane pictures are shown in the supplementary figure 1. **C)** Statistical evaluation of densitometry analysis (in Fiji) by T-test. N=3, black dots represent the range of measured values. ns = not significant. **** = p<0,0001.*

6.4 Confocal microscopy did not reveal any visible changes in the localization of LINC and LINC-related proteins in Prm2$^{-/-}$ mouse

To analyze, whether protein localization and posttranscriptional regulation is influenced by *Prm2* deletion, immunofluorescence microscopy of mouse tissue sections was done. At first, proteins of interest were co-stained with PNA. PNA binds to the outer acrosomal membrane, therefore staging of the seminiferous tubule spermiogenesis developmental phases is possible. Following proteins were visualized: LaminB2, LaminB2/3, SUN4, SUN3, ODF1, and KASH1. However, only LaminB2, LaminB2/3 and SUN4 were successfully visualized. The other antibodies failed to mark their proteins, even though different conditions and tissue processing methods were applied.

SUN4 was visualized only in postmeiotic stages of spermiogenesis with localization on the lateral posterior part of the sperm nucleus in both, WT and *Prm2*$^{-/-}$ mouse testes. No signal was detected in the region covered with acrosome or from the region of the implantation fossa (Fig. 12).

LmnB2 and LmnB2/3 were observed in both, somatic and postmeiotic testicular cells (Fig. 12 and Fig. 13, respectively). According to the literature, only LmnB3 should be present in maturating spermatozoa. Surprisingly, LmnB2 was present in the postmeiotic cells as well. Both proteins showed localization in both, the nuclear periphery and nucleoplasm located predominantly to the posterior part of the sperm nucleus.

LmnB2 can be found in the very posterior part of the maturating spermatid but is absent from the implantation fossa. In maturated spermatids, the signal was located within the manchette. The same pattern was observed in both, wild-type and *Prm2*$^{-/-}$ spermatids (Fig. 15).

After confirmation of localization of all proteins with PNA, colocalization studies were made. Both, LmnB2 and LmnB2/3 colocalize with SUN4 in both, WT and *Prm2*$^{-/-}$ and exhibit the same behavior (Fig. 14). It is important to note that none of the studied proteins was found in the cauda epididymis sperm.

As the LINC complex interacts with cytoskeletal proteins, their localization during spermiogenesis was examined as well. Confocal microscopy of mouse tests did not reveal any

significant changes in the localization of α-tubulin, α-tubulin acK40 (Fig. 10) β-actin and Septin12 (Fig. 16).

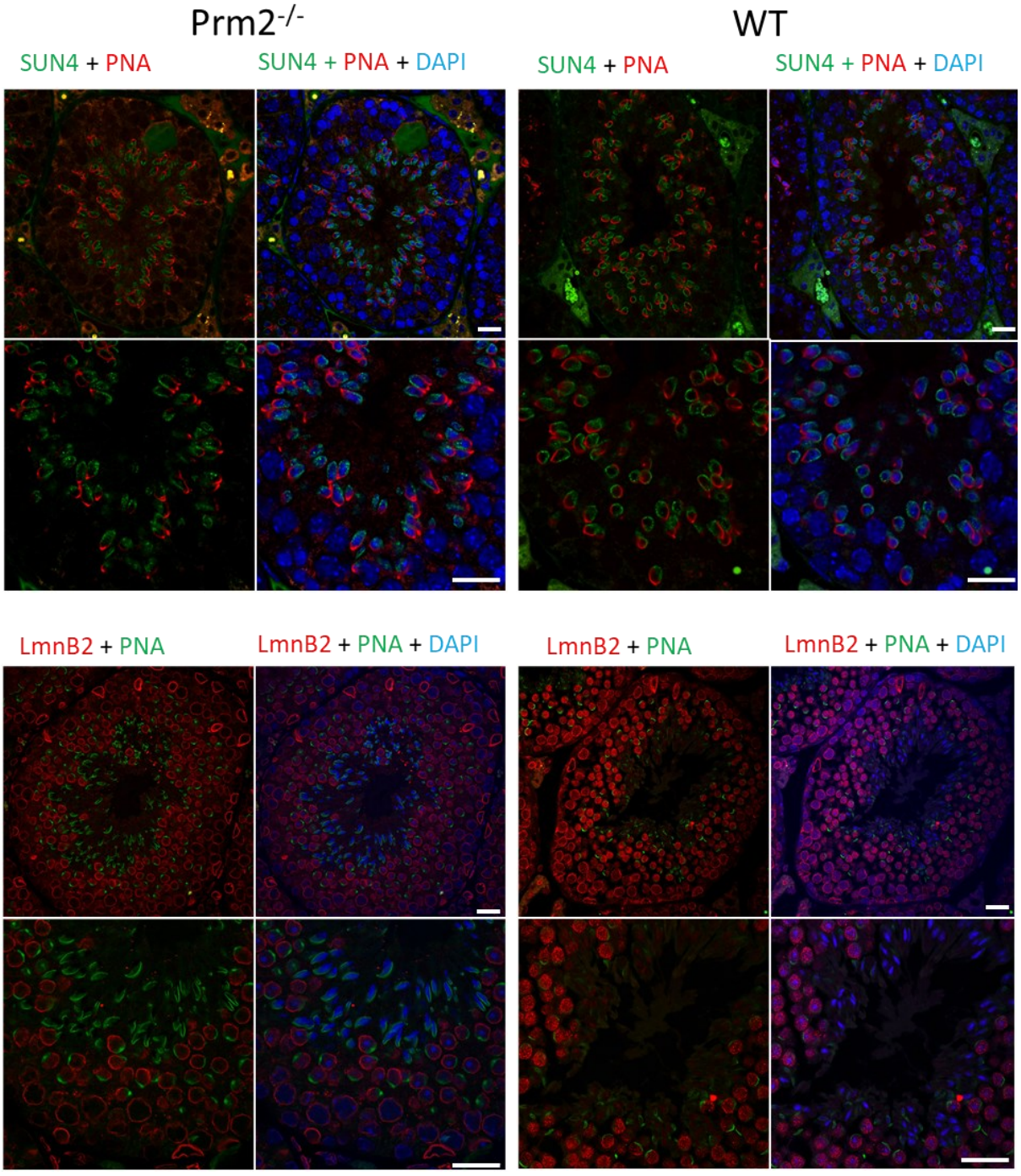

Figure 7: Colocalization of SUN4 with PNA and LaminB2 with PNA in Prm2$^{-/-}$ and WT testes. Paraffined testes sections, 5µm wide. Objective 63x, zoom 0,6 (top) and 1,2 (bottom). Scale bar = 20 µm.

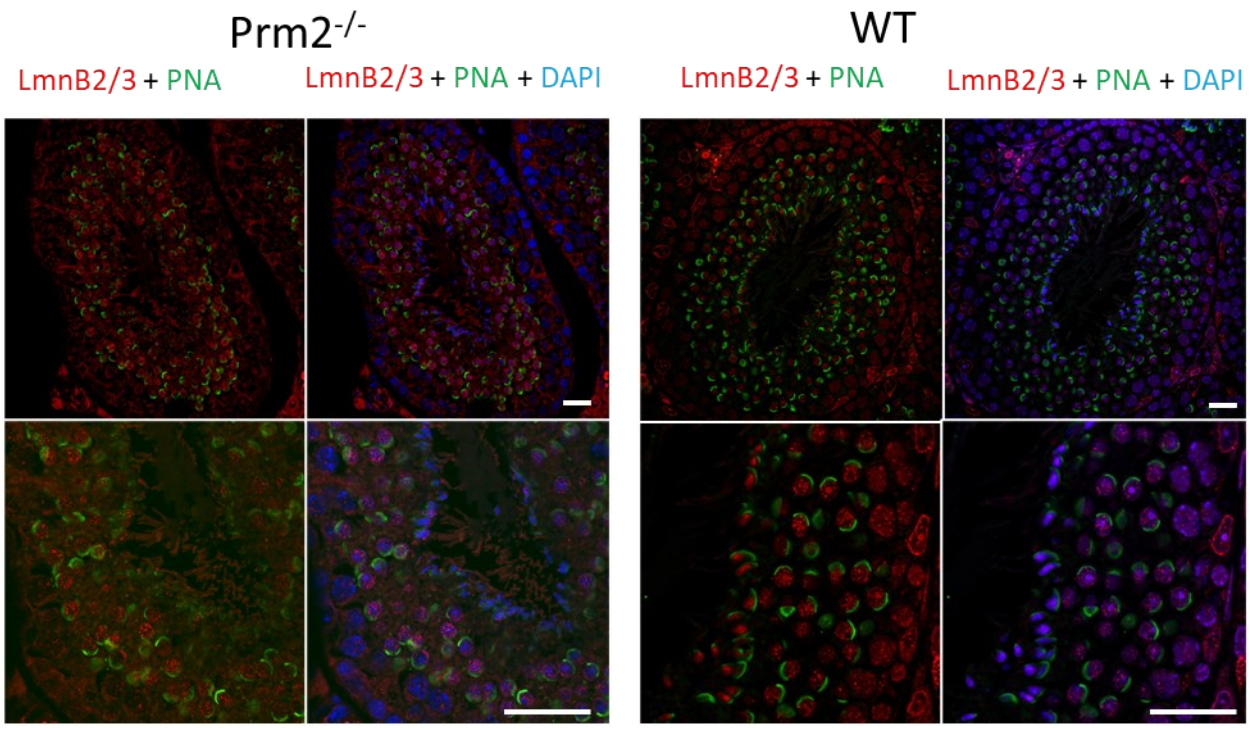

Figure 8: Colocalization of LaminB2/3 with PNA in Prm2$^{-/-}$ and WT testes. Paraffined testes sections, 5µm wide. Objective 63x, zoom 0,6 (top) and 1,2 (bottom). Scale bar = 20 µm.

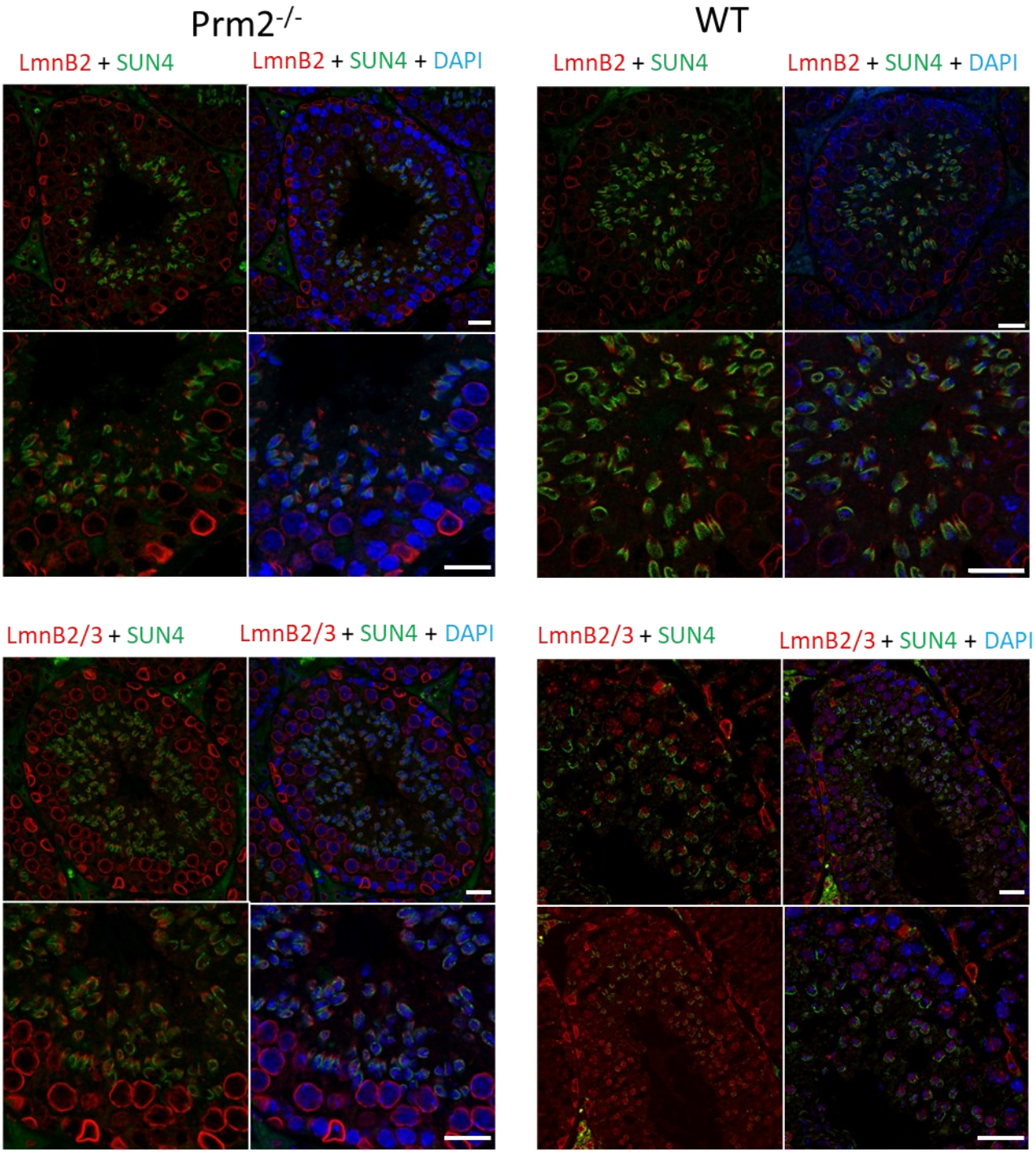

Figure 9: Colocalization of SUN4 with Lamin B2 and LaminB2/ in Prm2$^{-/-}$ and WT testes. Paraffined testes sections, 5µm wide. Objective 63x, zoom 0,6 (top) and 1,2 (bottom). Scale bar = 20 µm.

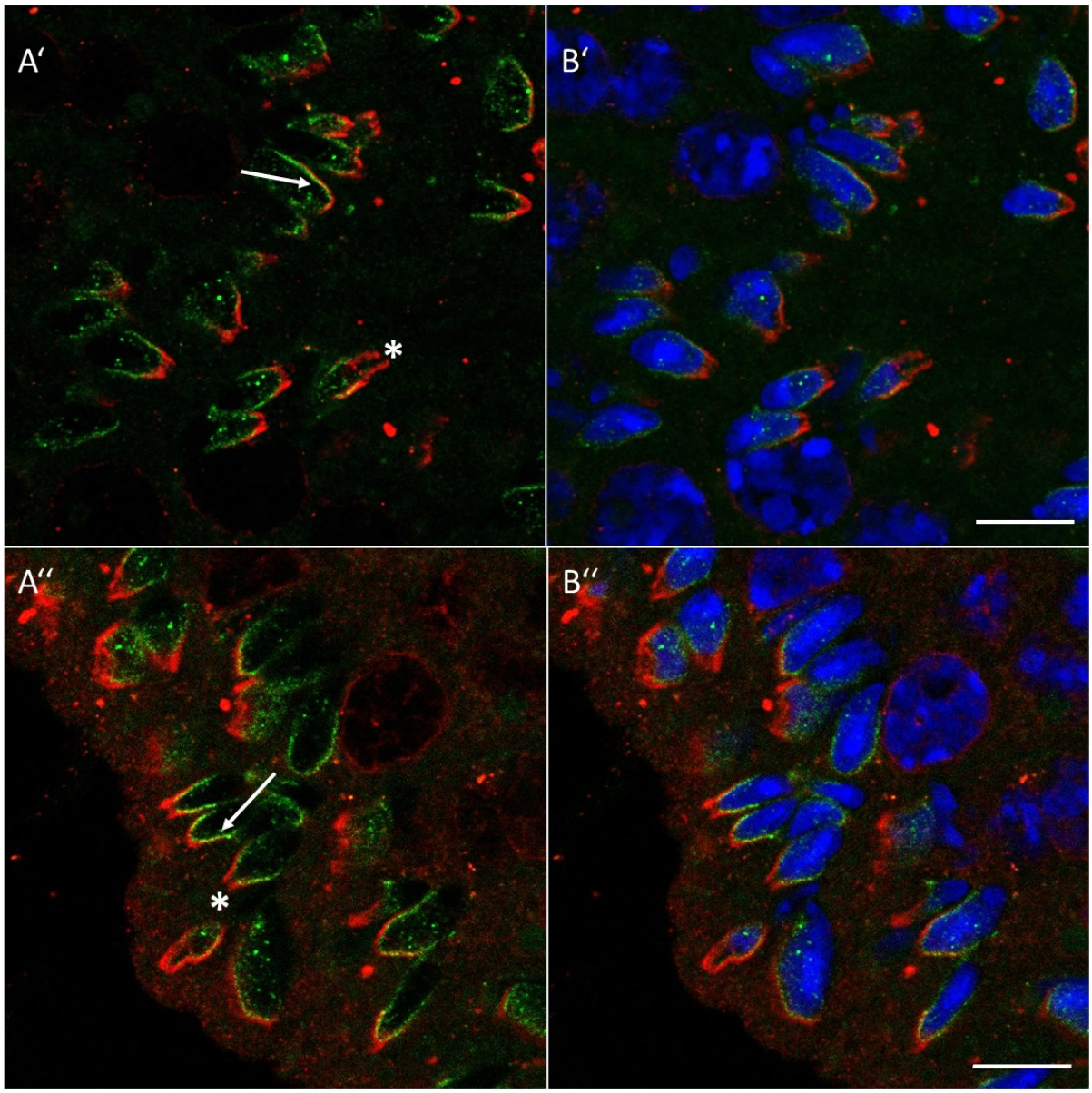

Figure 10: Detailed localization of Lamin B2 in the final stage of spermatid maturation colocalized with SUN4. Similar pattern is observed in Prm2$^{-/-}$ (dashed ‘) and wild-type (double dashed ‘‘), SUN4 is in green, Lamin B2 in red. Nuclei are stained blue. Arrow indicates colocalization of LaminB2 and SUN4, asterisk marks LaminB2 that is probably localized in the manchette. Scale bar = 10 µm.

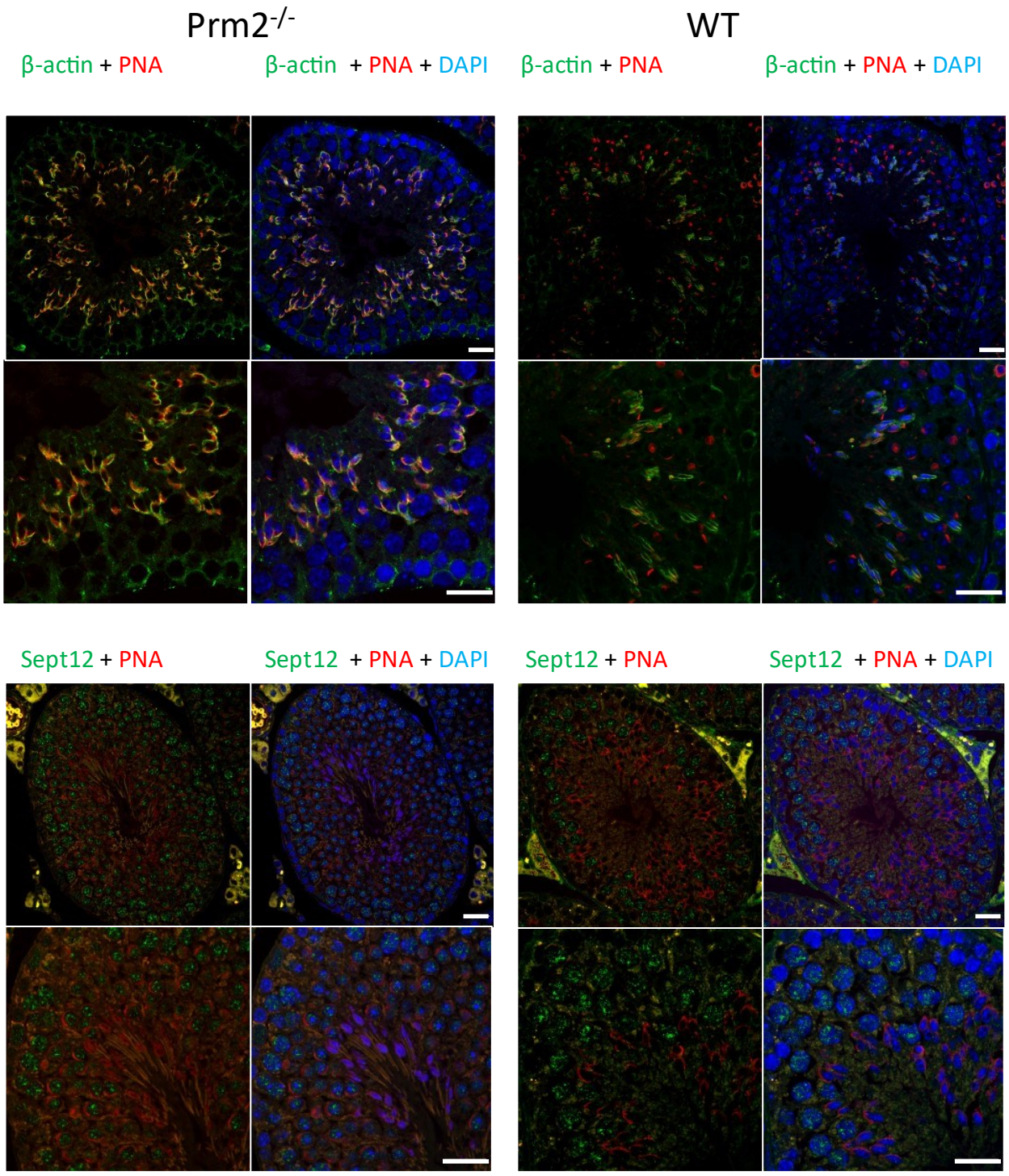

Figure 11: Localization of β-actin and Septin12 in Prm2$^{-/-}$ and WT testes. Paraffined testes sections, 5µm wide. Objective 63x, zoom 0,6 (top) and 1,2 (bottom). Scale bar = 20 µm.

6.5 Development of a new protocol for 3D microscopy analysis of individual seminiferous tubules based on the CLARITY method

To study the potential effect of *Prm2* deletion on mouse spermatogenesis *in situ* in 3D, the modified CLARITY (Chung *et al*., 2013) protocol was developed. The presented protocol enables us to study individual seminiferous tubule in detail. Moreover, compared to the original protocol, no transcardial perfusion is needed which makes the CLARITY method more accessible for students and people who are not skilled in mouse operations. For all parameters optimized, please see chapter 7.5.

1. Mouse testes were harvested, tunica albuginea was removed, and individual seminiferous tubules were isolated in a drop of PBS using fine tweezers.
2. STs were transferred to freshly prepared monomer solution and very gently stretched.
3. STs were incubated in the monomer solution for 2 hours at 4°C.
4. Monomer solution polymerization took place on a glass slide for 7 minutes in an N_2 atmosphere on a heat block preheated to 37°C. At first, a linear drop of gel monomer was applied on the glass slide, then a single ST was transferred into the individual drop of monomer matrix.
5. Polymerized samples were cleared in SDS buffer for 24 hours at 37°C with gentle orbital shaking (70 RPM).
6. STs were incubated in primary antibody diluted 1:100 in PBS + 10 % DMSO + 0,1 % Triton for 66 hours at RT with shaking 100 RPM.
7. Samples were washed in PBS 3x 2 hours at RT with orbital shaking at 100 RPM.
8. Secondary antibodies, PNA, DAPI, all diluted 1:500 in PBS + 10 % DMSO + 0,1 % Triton, were applied for 42 hours at RT with orbital shaking at 100 RPM in the dark.
9. Stained STs were washed in PBS 3x 2 hours at RT with orbital shaking at 100 RPM.
10. Samples were incubated in 80 % glycerol overnight at RT in the dark.
11. Samples were mounted into imaging chambers in the drop of fresh 80 % glycerol.

Please note that the time of staining and antibody dilutions may vary depending on the quality of the antibody. Timepoints here are optimized for antibody staining α-tubulin acK40.

The key steps of the protocol are illustrated by photos in the figure 17.

Microscopic data from STs prepared by the presented protocol can be obtained by the different microscope that is able to acquire images in Z projections (Z stacks). We have used a confocal

microscope (Carl Zeiss LSM 880 NLO), spinning disc (Nikon CSU-W1) and light sheet (Zeiss Lightsheet Z.1 microscope). The best images were obtained by Lighsheet and spinning disc microscopes. A confocal microscope from Zeiss was not able to obtain a signal from the distal part of the tubules, therefore incomplete data were obtained (Fig 18). Data obtained by spinning disc showed lover resolution quality compared to other microscopes, however, for Imaris analysis the resolution was sufficient. A big advantage of the spinning disc is its fast data acquisition. On the other hand, the best resolution is reached by using a Lighsheet microscope. Nevertheless, scanning takes serval hours, and the acquired dataset is very large.

To sum up, by the combination of Zstacks and Tile scan functions of the microscope, we were able to obtain a large amount of data, that provides new insight into sperm cell reshaping and development. Using appropriate staining, we can track different cell populations that correspond to particular stages of spermiogenesis.

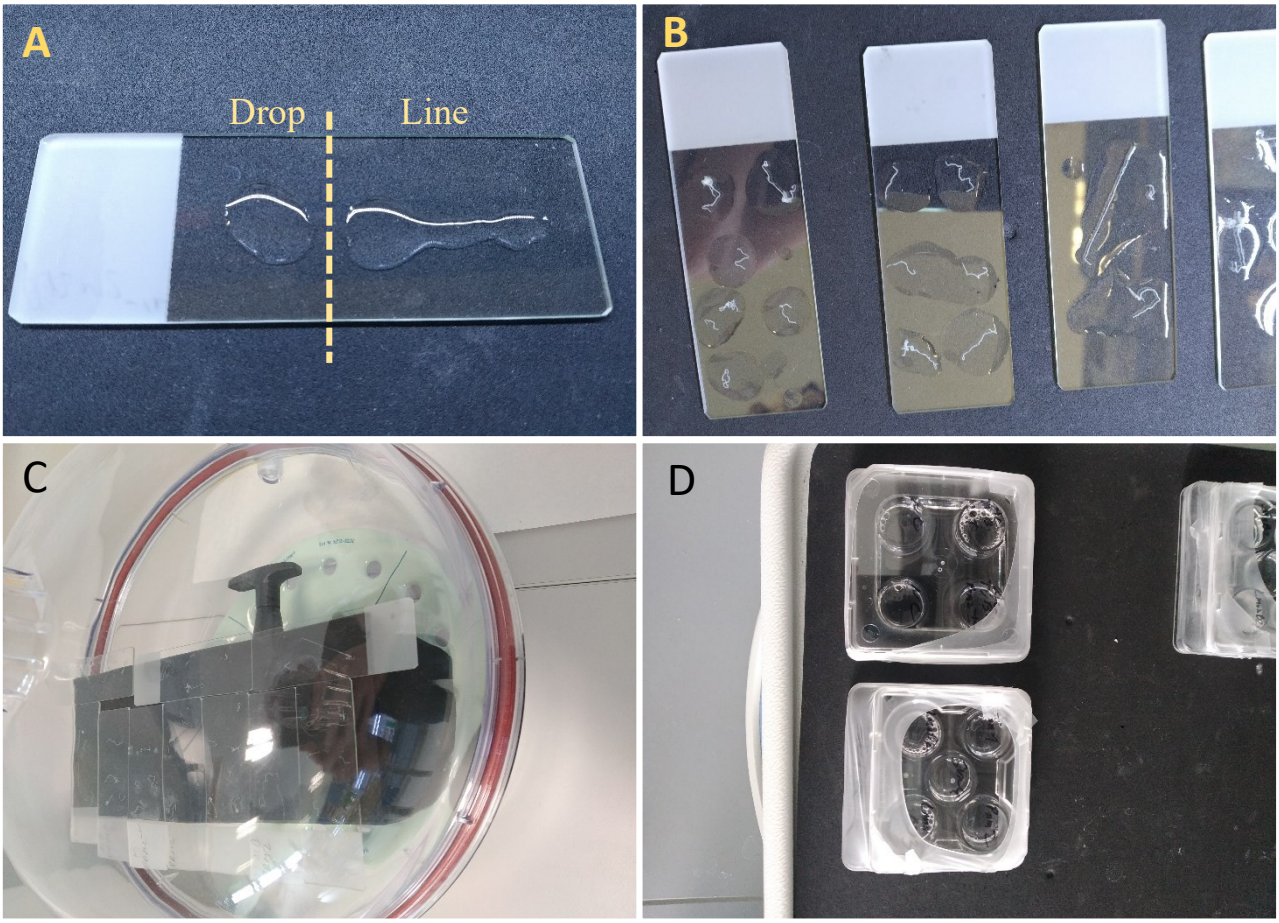

*Figure 12: Photos of key steps of the modified CLARITY protocol. **A)** Line shape of gel monomer is essential for proper STs embedding. **B)** example of embedded STs before gel polymerization. **C)** Gel polymerization setup: glass slides on heat block preheated to 37°C in exicator to maintain N_2 atmosphere. **D)** staining of STs took place in 4 or 5 flat bottom well dishes for in vitro cultivations.*

Table 10: Comparison of properties of data acquired by three different microscopes. The table shows time and raw dataset size. 1 individual seminiferous tubule Z projection was analysed without a Tile scan. Presented values are based on one representative example without any statistical analysis.

Microscope	Full ST scan?	Time (min)	Raw Data size (GB)
Carl Zeiss LSM 880 NLO	NO	45	1
Nikon CSU-W1	YES	5	4,75
Zeiss Lightsheet Z.1	YES	180	500

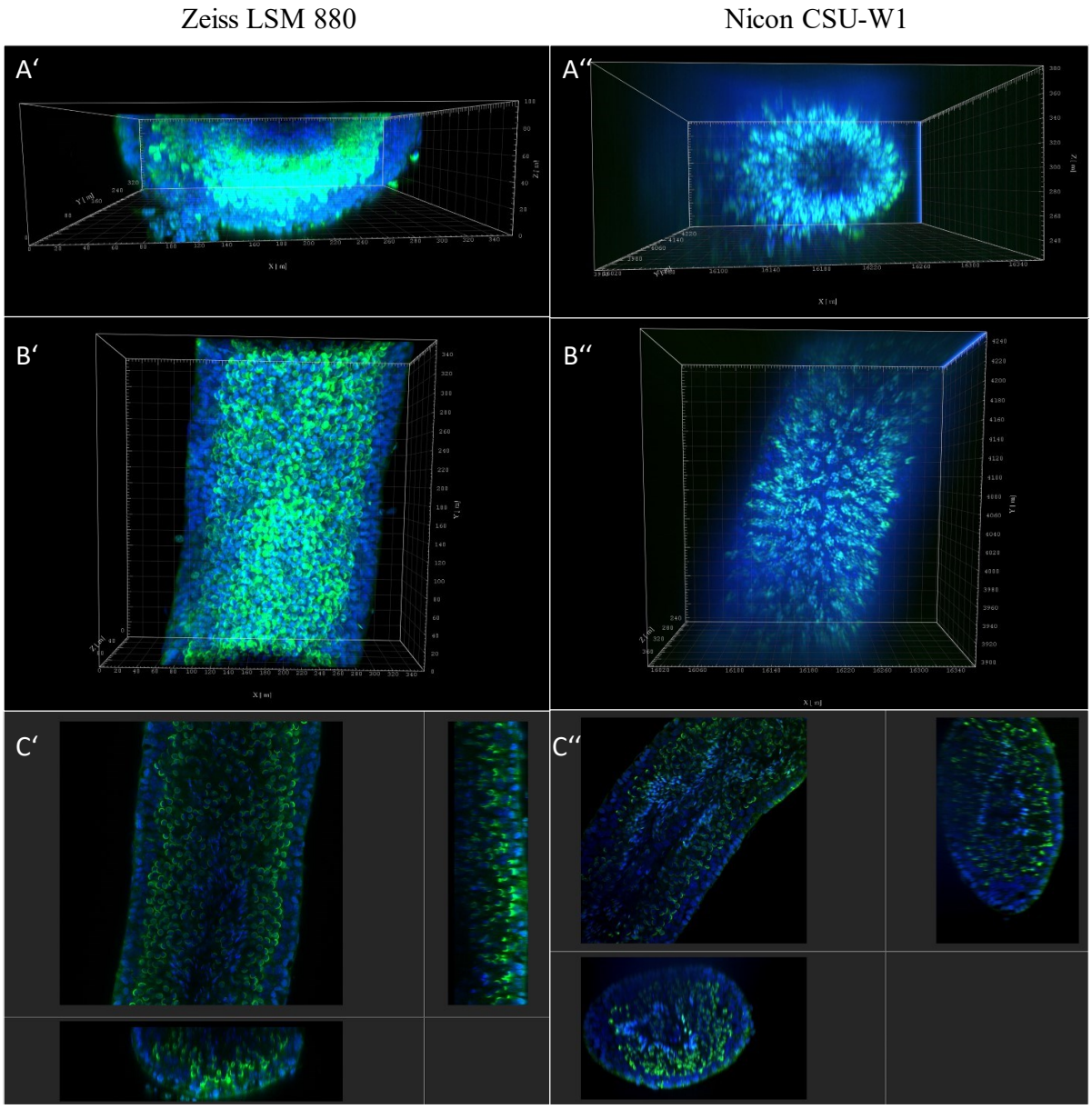

Figure 13: Comparison of data acquired by Confocal microscope Zeiss LSM 880 (dashed ‘) and Spinning disc Nicon CSU-W1 (double dashed ‘‘). Individual seminiferous tubule was stained with DAPI (blue) to mark nuclei and with PNA (green) to stain the acrosomes. ***A)*** *front view,* ***B)*** *top view,* ***C)*** *composition of the orthogonal plains.*

6.6 Modified CLARITY protocol revealed abnormal acrosome formation in *Prm2*$^{-/-}$ mouse

In the original publication (Schneider *et al.,* 2016) describing *Prm2*$^{-/-}$ mouse phenotype, the authors describe the process of spermiogenesis as unaffected. They also show, using PAS staining of mouse testes sections, that acrosome development is not influenced by *Prm2* deletion. However, using modified CLARITY protocol and Imaris software, we were able to show, that acrosome develops in an unphysiological way. Individual seminiferous tubule was stained with DAPI and PNA-AF488. Data were obtained using a confocal microscope and processed by Imaris software.

The acrosome of wild-type mice has a typical sickle-like shape, anchored to the anterior part of the nucleus, covering the whole topmost part of the nucleus. Therefore, the wild-type sperm cell looks optically longer. On the other hand, the acrosome of the *Prm2*$^{-/-}$ mouse is developing from the lateral part of the sperm, resembling a branching tree. The acrosome is also absent from the topmost anterior part of the nucleus (Fig. 20). Also, the nuclear-acrosomal transition in WT is smooth, meanwhile, the boundary in the *Prm2*$^{-/-}$ sperm is not so obvious. Moreover, the cytoplasm of the *Prm2*$^{-/-}$ seems to contain a larger amount of acrosomal vesicles than the WT (Fig. 21).

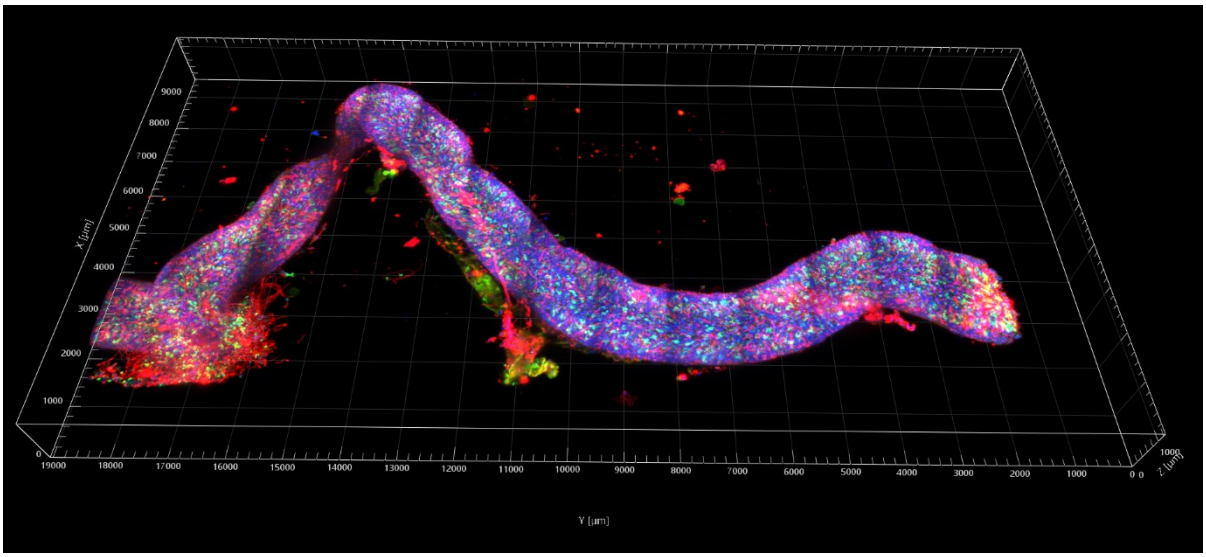

Figure 19: Representative example of Seminiferous tubule data from Lightsheet microscope. Data were obtained by the combination of Z stacks and Tile scan. Nuclei are in blue, acrosomes in green and α-tubulin acK40 is in red.

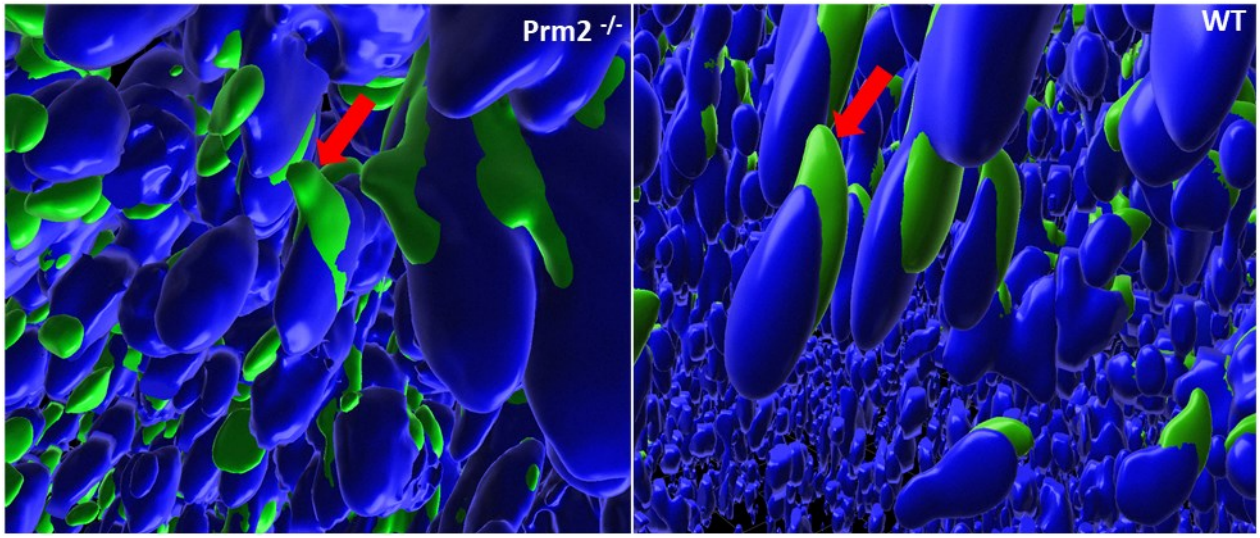

Figure 140: Representative image of acrosome development. Data were obtained using Zeiss LSM 880 microscope and Z stacks were rendered and processed in Imaris software. Acrosomes are shown in green, nuclei are in blue. The red arrow indicates developing acrosome.

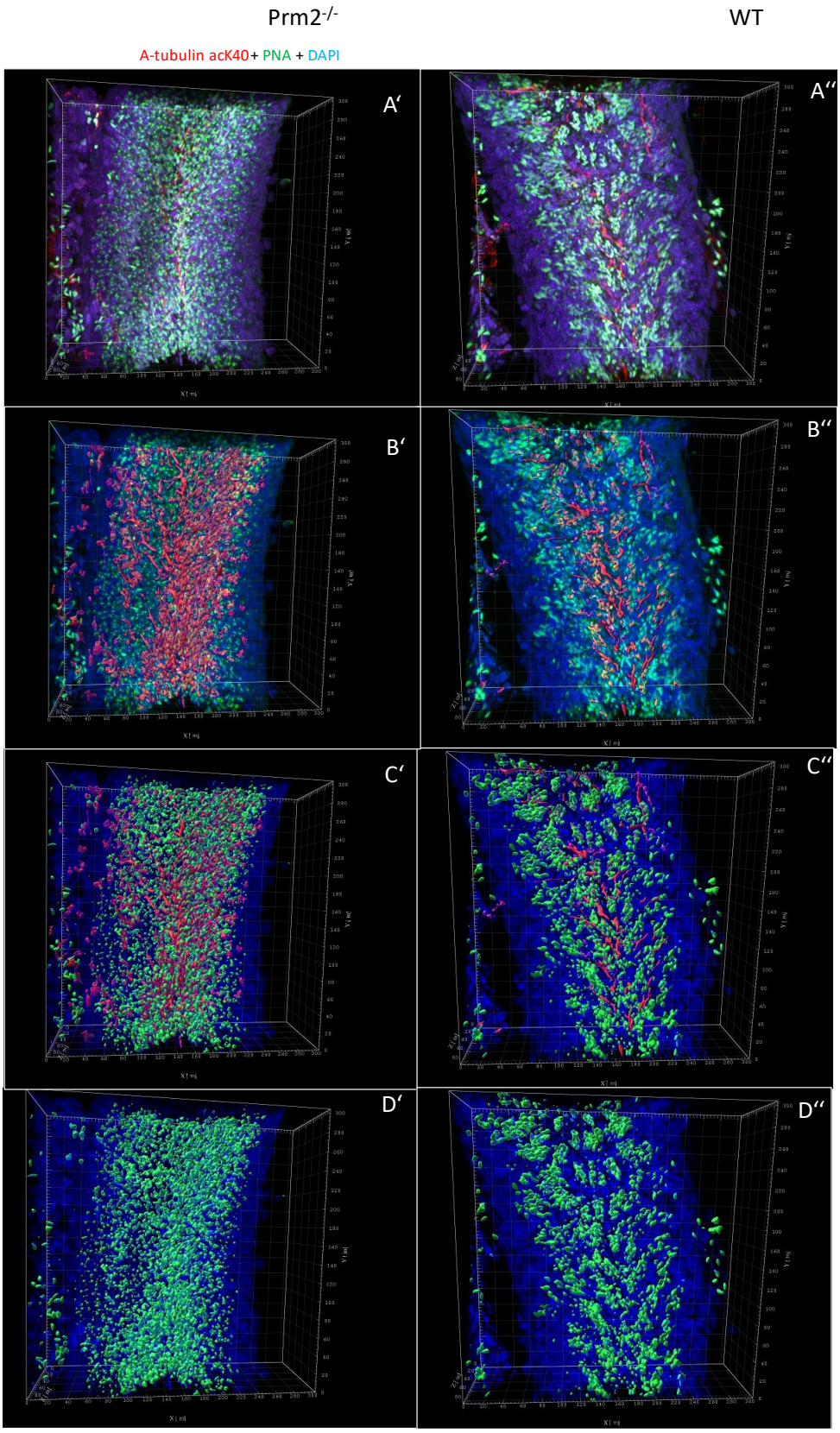

Figure 21: Representative examples of stained individual seminiferous tubules for α-tubulin acK40 (red), PNA (green), and Nuclei (blue) from Prm2$^{-/-}$ (dashed ‘) and wild-type (double dashed ‘‘) prepared by novel CLARITY workflow. Data were obtained on Zeiss LSM 880 using Zstacks and processed in Imaris. A) Z stacks in 3D projecting without rendering, B) α-tubulin acK40 rendered, C) α-tubulin acK40 and PN rendered. D) show just PNA with nuclei to demonstrate a higher number of proacrosomal vesicles in Prm2$^{-/-}$ ST.

7 Discussion

Infertility is a worldwide phenomenon that affects about 15 % of couples (Sharlip *et al*., 2002). Male factors contribute to infertility by approximately 50 %. About half of infertile men have an unknown origin, so-called "Idiopathic infertility", and the proper treatment is unclear (Jung and Seo 2014). The ratio of *PRM1* to *PRM2* mRNA in human sperm and its correlation with decreased fertility has been studied since 2001 (Steger *et al*., 2001). It was shown, that *PRM1* : *PRM2* mRNA in human ejaculated sperm is 1 and may vary from 0,92 to 1,08 (Steger *et al*., 2008). Since that, unphysiological levels of sperm protamination were linked to male infertility as patients with a lower ratio (0,81) of *PRM1* and *PRM2* mRNA have decreased sperm motility as well as progressive motility. Furthermore, patients with a decreased ratio (0,61) of *PRM1* and *PRM2* mRNA were linked to have a negative impact on early embryonic development with a higher occurrence of unexplained recurrent miscarriage, probably caused by increased fragmentation of sperm DNA (Rogenhofer *et al*., 2017).

In this study, the *Prm2*$^{-/-}$ mouse line was further characterized. Sperm of *Prm2*$^{-/-}$ mice have, besides the other defects, fully immotile sperm. The molecular mechanism behind this phenotype has not been yet understood (Schneider *et al.*, 2016, Schneider *et al*., 2020), and was the aim of my thesis. Even though sperm nucleus packaging with histone replacement and sperm motility seems to be two distant events, the *Prm2*$^{-/-}$ phenotype suggests their interconnection. Both events are associated with cytoskeleton and cytoskeletal motors interplay. Moreover, both events can be influenced by different modifications such as (de)acetylation. Therefore, we have focused on the analysis of the Linker of Nucleoskeleton and Cytoskeleton, the so-called LINC complex which provides mechanical connection and signals transduction from the nucleoskeleton to the cytoskeleton and vice versa.

We aimed to compare the integrity of the LINC complex and its binding partners in WT and *Prm2*$^{-/-}$ mice during the spermiogenesis. Special focus was put on SUN proteins, due to the fact that sperm of *Sun4*$^{-/-}$ mice have flagellum bend around their head (Pasch *et al*., 2015), which resembles the phenotype of *Prm2*$^{-/-}$ sperm. Further, it was shown that *Sun3* deletion in mice is associated with abnormal acrosome formation (Gao *et al*., 2020). Moreover, these two SUN proteins are known to form LINC complex with KASH1 and also to interact with LaminB1 (Yeh *et al*., 2015) as crucial linkers between cytoskeleton and nucleoskeleton. Additionally, SUN3: SUN4: KASH1 LINC complex is located on the posterior part of the sperm head, therefore the complex is crucial for head-to-tail communication. For these reasons, this

multiprotein complex represents a structure with the potential to be highly influenced by *Prm2* deletion.

At first, analysis of gene expression of the LINC and LINC-related genes did not reveal any significant change in levels of testicular mRNA in *Prm2*$^{-/-}$ compared to wild type. As protein localization but not gene expression might be influenced by the *Prm2* deletion, localization of the same proteins using a confocal microscope was traced. Here, many different conditions were applied but antibodies against SUN3 and KASH1 failed to mark their targets. Therefore, only LaminB2, Lamin B2/3 and SUN4 were localized in the mouse testes sections. Currently, there is no viable antibody against LaminB3 specifically. From the pictures (Fig: 12, 13, 14). obtained by the confocal microscope the localization of LaminB2, Lamin B2/3 and SUN4 was not changed in *Prm2*$^{-/-}$ testes compared to WT. Importantly, however, we achieved to visualize LaminB2 in postmeiotic spermatids in the stages of their final maturation (Fig: 15). This phenomenon has not been documented yet and this finding is supported by the study (Elkhatib *et al*., 2014), showing that the Lamin B2 is present on some human ejaculated sperm.

Due to the fact that spermiogenesis is a dynamic process that involves a lot of cellular reshaping, capturing sperm formation *in situ* is crucial for data analysis. Even though the CLARITY (Chung *et al*., 2013) method allows to prepare of samples of desired quality, in order to track different cell populations in an individual seminiferous tubule the precise modification of the generally used protocol was required. We achieved to establish a new protocol and this newly developed workflow enabled us to stain individual cells and monitor spermiogenesis step by step. Moreover, this protocol is also compatible with antibody staining, therefore changes in space and time of desired protein can be tracked. Using this custom-modified CLARITY protocol, the abnormal shaping of acrosomes was observed. The aberrant acrosome shaping is in contrast with the original publication describing the *Prm2*$^{-/-}$ phenotype (Schneider *et al*., 2016). Here authors analyzed acrosomal formation using the traditional approach – analysis of tissue sections stained by Periodic acid–Schiff staining which did not reveal any difference.

The aberrant acrosomal formation was recently associated with defects in cytoskeletal motor proteins. For example, the study made on Snell's waltzer mice deficient in myosin VI, MYO6, showed, that these mice have reduced fertility and degenerated neurosensory epithelium of the inner ear. Detailed analysis of the spermiogenesis revealed that after MYO6 depletion the acrosome is delocalized since the Cap phase and the cytoplasm contains a larger amount of proacrosomal vesicles. It seems that MYO6 leads the docking of acrosomal vesicles to the

natural position. In the absence of MYO6, the acrosome is developed on the lateral part of the spermatid (Zakrzewski *et al*., 2020). Another evidence of the importance of cytoskeletal motor proteins in the acrosomal formation was brought by She *et al*. in 2021 describing that the aberrant acrosome was developed after inhibition of kinesins-7 CENP-E. Particularly, the acrosome is asymmetrical, the cytoplasm contains acrosomal vesicles, and the forming acrosome is not located on the anterior part of the sperm head but is tilled to the side. Both, sperm with depleted MYO6 or with inhibited CENP-E, have a similar phenotype to the *Prm2*$^{-/-}$ testicular sperm. Taken together, results from these studies and our observation suggest that cytoskeletal motor proteins might be disrupted and negatively influence acrosomal formation during the spermiogenesis in the *Prm2*$^{-/-}$ mouse and we will carry on investigating this possibility.

On top of that, the microscopic data also revealed a discrepancy in the pattern of tubulin acetylation at lysine 40. It became clear that α-tubulin in *Prm2*$^{-/-}$ sperm was acetylated in the whole tail, meanwhile, in the WT, the acetylation signal was observed only in the midpiece and endpiece of the tail (Fig: 9). Control staining for the α-tubulin did not reveal any changes in the signal distribution. Therefore, we concluded that tubulin dynamics is not influenced by the *Prm2* deletion. On the other hand, the clear difference in the pattern of α-tubulin acK40 in WT and *Prm2*$^{-/-}$ sperm might imply a disbalance in the activity of αTAT1, HDAC6 or in any other MAP (Bhagwat *et al*., 2014, Chawan *et al*., 2020) and needs to be further addressed. Importantly, the densitometric analysis did not show a significant difference in the abundance of α-tubulin acK40 in wild-type and *Prm2*$^{-/-}$ sperm, therefore it could be concluded that *Prm2*$^{-/-}$ sperm may have different localization, but the similar abundance of the α-tubulin acK40 compared to the WT. As the pattern of α-tubulin localization as well as protein abundance are consistent in WT and *Prm2*$^{-/-}$ sperm, it might imply that axonemal polymerization was not influenced, merely the tubulin acetylation pattern was different.

In order to cover all of cytoskeletal proteins status, the abundance of β-actin, α-tubulin and β-tubulin was analyzed. Interestingly, there was discovered a significant increase in the protein level of β-actin ($p<0,0001$) in *Prm2*$^{-/-}$ sperm. In the contrast, the relative gene expression of *ActB* was significantly decreased ($p<0,01$) in *Prm2*$^{-/-}$ mouse testes. β-actin is known to be located in the acroplaxome of developing sperm, therefore it is expected to play a yet undefined role in the acrosome formation (Kierszenbaum and Tres, 2004). Further, testis-specific actin capping protein CPβ3 is known to be abnormally regulated in human patients with oligozoospermia and asthenozoospermia. During spermiogenesis, this testis-specific protein is

located in the acrosome region and the manchet. In maturated sperm, CPβ3 is located only in the postacrosomal region (Soda *et al*., 2017) suggesting an important role of β-actin during the spermiogenesis. Another role of the actin capping proteins was shown in experiments using Murrah buffalo sperm. Here, expression of F-actin-capping protein subunit bet (CAPZB) and tektin 2 were analyzed in sperm with high and low motility. Both proteins promote sperm motility. CAPZB causes actin depolymerization by binding to the barbed end and capping the actin filament, meanwhile tektins provide stability to axonemal microtubules. It was found that the expression of both genes is significantly lower in sperm with low motility (Xiong *et al*., 2018). The role of β-actin in spermiogenesis was also studied in the mouse model of *Sun4*$^{-/-}$, where β-actin located in the manchette was able to polymerize but failed to assemble in the physiological way. The actin filaments were disorganized and were distant from the NE. The actin rod-like filaments were also absent from the acrosomal region of *Sun4*$^{-/-}$ spermatids (Pasch *et al*.,2015). Taken together with the data obtained so far, β-actin seems to be a possible protein candidate which could be dysregulated in the *Prm2*$^{-/-}$ mouse, by so far an unknown mechanism. However, this hypothesis needs to be further verified.

To summarize the finding as the outcome of this thesis, the phenotype of the *Prm2*$^{-/-}$ mouse was further characterized with a focus on the LINC and LINC-related proteins. Experiments that were performed so far did not reveal clear differences between WT and *Prm2*$^{-/-}$ mouse LINC components (SUN and KASH proteins) or LaminB (the nuclear partner of the LINC), on the level of gene expression and protein localization in the testes. However, significant changes were detected in the gene expression and protein abundance of β-actin but not in the other cytoskeletal proteins. Taken together with data from the newly modified CLARITY protocol, which showed a defective acrosome formation and a large amount of proacrosomal vesicles during the spermiogenesis, it is possible that β-actin dynamics in *Prm2*$^{-/-}$ sperm are dysregulated as well as the function of cytoskeletal motor proteins. β-actin stabilization might serve as a scaffolding, trying to keep the acrosome attached to the sperm head with reflect to deformations connected with *Prm2*$^{-/-}$ emerged during epididymal maturation. However, these hypotheses need further investigation for example by super resolution microscopy using specific antibodies against nuclear actin. Further, microscopic data revealed redistribution of α-tubulin acK40, specifically in sperm of *Prm2*$^{-/-}$ mouse, tubulin was detected to be acetylated in the whole tail length, meanwhile in the WT sperm, in particularly defined regions. Our data, therefore, allowed us to modify the original theory and hypothesis that it is not the LINC complex but cytoskeleton-related pathologies which lead to the loss of sperm motility in *Prm2*$^{-/-}$ mouse.

8 Conclusion

In this thesis, LINC complex proteins and LINC-related proteins were examined in WT and *Prm2*$^{-/-}$ mouse line.

Ad aim 1: Localization of LaminB2, Lamin B2/3, SUN4, Septin12, α-tubulin, α-tubulin acK40 and β-actin was examined on paraffined testes sections and it was not influenced by the *Prm2* deletion. Importantly, new localization of LmnB2 was discovered in the postmeiotic stages of spermatogenesis. Discrepancies in the localization of α-tubulin acK40 in mouse sperm were found in the *Prm2*$^{-/-}$.

Ad aim 2: Gene expression of *Sun3, Sun4, Kash1, LmnB2, LmnB3, LmnB2/3, ActB, Tub5A, Tub5B, and Sept12* in testicular cells was analyzed and *ActB* and *Sept12* had significantly decreased ($p < 0,05$).

Deliverables of the thesis:

1. I was able to modify and optimize the CLARITY protocol so that we are now able to study spermatogenic processes in individual seminiferous tubule *in situ* in 3D.

2. Using our newly developed protocol abnormal acrosome formation was observed in the *Prm2*$^{-/-}$ seminiferous tubule (Fig. 20).

3. Changes in the pattern of α-tubulin acetylation at lysine 40 in *Prm2*$^{-/-}$ sperm were described (Fig. 9).

4. Surprising increase in β-actin abundance in *Prm2*$^{-/-}$ was observed (Fig 11).

Taken together, this thesis further characterized *Prm2*$^{-/-}$ mouse line and brings up some ideas for follow-up studies. During my Ph.D. studies, I will continue in this project with the following goals:

1. To study the cytoskeletal motor proteins and their involvement in acrosome formation.

2. To study the dynamics of α-tubulin (de)acetylation in sperm.

9 Literature

Alsheimer M., Benavente R. (1996): Change of karyoskeleton during mammalian spermatogenesis: expression pattern of nuclear lamin C2 and its regulation. Exp Cell Res.;228(2):181-188.

Ammer H., Henschen A., Lee C.H. (1986): Isolation and amino-acid sequence analysis of human sperm protamines P1 and P2. Occurrence of two forms of protamine P2. Biol Chem Hoppe Seyler 367(6): 515-522.

Balhorn R. (1982): A model for the structure of chromatin in mammalian sperm. J Cell Biol 93(2): 298-305.

Bhagwat S., Dalvi V., Chandrasekhar D., Matthew T., Acharya K., Gajbhiye R., Kulkarni V., Sonawane S., Ghosalkar M., Parte P. (2014): Acetylated α-tubulin is reduced in individuals with poor sperm motility. Fertil Steril.;101(1):95-104.e3.

Breitbart H., Cohen G., Rubinstein S. (2005): Role of actin cytoskeleton in mammalian sperm capacitation and the acrosome reaction. Reproduction 129(3): 263-268.

Brener E., Rubinstein S., Cohen G., Shternall K., Rivlin J., Breitbart H. (2003): Remodeling of the actin cytoskeleton during mammalian sperm capacitation and acrosome reaction. Biol Reprod 68(3): 837-845.

Brunner A. M., Nanni P., Mansuy I. M. (2014): Epigenetic marking of sperm by post-translational modification of histones and protamines. Epigenetics Chromatin.20;7(1):2.

Burgos M. H., Fawcett D. W. (1955): Studies on the fine structure of the mammalian testis. I. Differentiation of the spermatids in the cat (Felis domestica). J Biophys Biochem Cytol 1(4): 287-300.

Sharlip I. D., Jarow J. P., Belker A. M., Lipshultz L. I., Sigman M., Thomas A. J., Schlegel P. N., Howards S. S., Nehra A., Damewood M. D., Overstreet J. W., Sadovsky R. (2002): Best practice policies for male infertility. Fertil Steril.;77(5):873-82.

Chawan V., Yevate S., Gajbhiye R., Kulkarni V., Parte P. (2020): Acetylation/deacetylation and microtubule associated proteins influence flagellar axonemal stability and sperm motility. Biosci Rep.;40(12): BSR20202442.

Cho C., Jung-Ha H., Willis W. D., Goulding E. H., Stein P., Xu Z., Schultz R. M., Hecht N. B., Eddy E. M. (2003): Protamine 2 deficiency leads to sperm DNA damage and embryo death in mice. Biol Reprod 69(1): 211-217.

Chung K., Wallace J., Kim S. Y., Kalyanasundaram S., Andalman A. S., Davidson T. J., Mirzabekov J. J., Zalocusky K. A., Mattis J., Denisin A. K., Pak S., Bernstein H., Ramakrishnan C., Grosenick L., Gradinaru V., Deisseroth K. (2013): Structural and molecular interrogation of intact biological systems. Nature 497(7449): 332-337.

Coelingh J. P., Rozijn T. H., Monfoort C. H. (1969): Isolation and partial characterization of a basic protein from bovine sperm heads. Biochim Biophys Acta 188(2): 353-356.

Cornwall G. A. (2009): New insights into epididymal biology and function. Hum Reprod Update.;15(2):213-27.

Corzett M., Mazrimas J., Balhorn R. (2002): Protamine 1: protamine 2 stoichiometry in the sperm of eutherian mammals. Mol Reprod Dev 61(4): 519-527.

Coutton C., Escoffier J., Martinez G., Arnoult C., Ray P. F. (2015): Teratozoospermia: spotlight on the main genetic actors in the human. Hum Reprod Update.;21(4):455-485.

Ding X., Xu R., Yu J., Xu T., Zhuang Y., Han M. (2007): SUN1 is required for telomere attachment to nuclear envelope and gametogenesis in mice. Dev Cell.;12(6):863-872.

Dunleavy J. E. M., O'Bryan M. K., Stanton P. G., O'Donnell L. (2019): The cytoskeleton in spermatogenesis. Reproduction 157(2): R53-R72.

Elkhatib R., Longepied G., Paci M., Achard V., Grillo J-M., Levy N., Mitchell M. J,. Metzler-Guillemain C. (2014): Nuclear envelope remodelling during human spermiogenesis involves somatic B-type lamins and a spermatid-specific B3 lamin isoform. Molecular Human Reproduction 21(3): 225-236.

Finkelstein M., Etkovitz N., Breitbart H. (2010): Role and regulation of sperm gelsolin prior to fertilization. J Biol Chem 285(51): 39702-39709.

Firmbach-Kraft I., Stick R. (1995): Analysis of nuclear lamin isoprenylation in Xenopus oocytes: isoprenylation of lamin B3 precedes its uptake into the nucleus. J Cell Biol.;129(1):17-24.
Freitas M. J., Vijayaraghavan S., Fardilha M. (2016): Signaling mechanisms in mammalian sperm motility†. Biology of Reproduction 96(1): 2-12.
Furukawa K., Hotta Y. (1993): cDNA cloning of a germ cell specific lamin B3 from mouse spermatocytes and analysis of its function by ectopic expression in somatic cells. Embo j 12(1): 97-106.
Gao Q., Khan R., Yu C., Alsheimer M., Jiang X., Ma H., Shi Q. (2020): The testis-specific LINC component SUN3 is essential for sperm head shaping during mouse spermiogenesis. J Biol Chem 295(19): 6289-6298.
Gatewood J. M., Cook G. R., Balhorn R., Bradbury E. M., Schmid C. W. (1987): Sequence-specific packaging of DNA in human sperm chromatin. Science 236(4804): 962-964.
Göb E., Schmitt J., Benavente R., Alsheimer M. (2010): Mammalian sperm head formation involves different polarization of two novel LINC complexes. PLoS One 5(8): e12072.
Gurusaran M., Davies O. R. (2021): A molecular mechanism for LINC complex branching by structurally diverse SUN-KASH 6:6 assemblies. Elife 10.
Haque F., Lloyd D. J., Smallwood D. T., Dent C. L., Shanahan C. M., Fry A. M., Trembath R. C., Shackleton S. (2006) SUN1 interacts with nuclear lamin A and cytoplasmic nesprins to provide a physical connection between the nuclear lamina and the cytoskeleton. Mol Cell Biol.;26(10):3738-51
Horn H. F., Kim D. I., Wright G. D., Wong E. S., Stewart C. L., Burke B., Roux K. J. (2013): A mammalian KASH domain protein coupling meiotic chromosomes to the cytoskeleton. J Cell Biol 202(7): 1023-1039.
Houben F., Ramaekers F. C., Snoeckx L. H., Broers J. L. (2007): Role of nuclear lamina-cytoskeleton interactions in the maintenance of cellular strength. Biochim Biophys Acta.;1773(5):675-686.
Hubbert C., Guardiola A., Shao R., Kawaguchi Y., Ito A., Nixon A., Yoshida M., Wang X. F., Yao T.P. (2002): HDAC6 is a microtubule-associated deacetylase. Nature.23;417(6887):455-8.
Ickowicz D., Finkelstein M. and Breitbart H. (2012): Mechanism of sperm capacitation and the acrosome reaction: role of protein kinases. Asian J Androl 14(6): 816-821.
Ihara M., Kinoshita A., Yamada S., Tanaka H., Tanigaki A., Kitano A., Goto M., Okubo K., Nishiyama H., Ogawa O., Takahashi C., Itohara S., Nishimune Y., Noda M., Kinoshita M. (2005): Cortical organization by the septin cytoskeleton is essential for structural and mechanical integrity of mammalian spermatozoa. Dev Cell.;8(3):343-52.
Inaba K. (2003): Molecular architecture of the sperm flagella: molecules for motility and signaling. Zoolog Sci.;20(9):1043-56.
Castañeda J. M., Miyata H., Ikawa M., Matzuk M. M. (2018): Sperm Defects, Academic press, ISBN 9780128151457, Pages 276-281.
Jung J. H., Seo J. T. (2014): Empirical medical therapy in idiopathic male infertility: Promise or panacea? Clin Exp Reprod Med 41(3): 108-114.
Khawar M. B., Gao H., Li W. (2019): Mechanism of Acrosome Biogenesis in Mammals. Front Cell Dev Biol 7: 195.
Kierszenbaum A. L., Rivkin E., Tres L. L. (2003): Acroplaxome, an F-Actin–Keratin-containing Plate, Anchors the Acrosome to the Nucleus during Shaping of the Spermatid Head. Molecular Biology of the Cell 14(11): 4628-4640.
Kierszenbaum A. L., Rivkin E., Tres L. L., Yoder B. K., Haycraft C. J., Bornens M., Rios R. M. (2011) GMAP210 and IFT88 are present in the spermatid golgi apparatus and participate in the development of the acrosome-acroplaxome complex, head-tail coupling apparatus and tail. Dev Dyn;240(3):723-736.
Kierszenbaum A. L., Tres L. L., Rivkin E., Kang-Decker N., van Deursen J. M. A (2004): The Acroplaxome Is the Docking Site of Golgi-Derived Myosin Va/Rab27a/b-Containing Proacrosomal Vesicles in Wild-Type and Hrb Mutant Mouse Spermatids1. Biology of Reproduction 70(5): 1400-1410.
Kierszenbaum A. L., Tres L. L. (2004): The acrosome-acroplaxome-manchette complex and the shaping of the spermatid head. Arch Histol Cytol.;67(4):271-84.

Kmonickova V., Frolikova M., Steger K., Komrskova K. (2020): The Role of the LINC Complex in Sperm Development and Function. Int J Mol Sci.28;21(23):9058.
Kuo P. L., Chiang H. S., Wang Y. Y., Kuo Y. C., Chen M. F., Yu I. S., Teng Y. N., Lin S. W., Lin Y. H. (2013): SEPT12-microtubule complexes are required for sperm head and tail formation. Int J Mol Sci. 7;14(11):22102-16.
Larson J. L., Miller D. J. (1999): Simple histochemical stain for acrosomes on sperm from several species. Mol Reprod Dev 52(4): 445-449.
Lehti M. S., Sironen A.(2016): Formation and function of the manchette and flagellum during spermatogenesis. Reproduction.;151(4):R43-R54
Lei K., Zhu X., Xu R., Shao C., Xu T., Zhuang Y., Han M. (2012): Inner nuclear envelope proteins SUN1 and SUN2 play a prominent role in the DNA damage response. Curr Biol. Sep 11;22(17):1609-15.
Lin Y. H., Chou C. K., Hung Y. C., Yu I. S., Pan H. A., Lin S. W., Kuo P. L. (2011) SEPT12 deficiency causes sperm nucleus damage and developmental arrest of preimplantation embryos. Fertil Steril. ;95(1):363-5.
Lin Y. H., Lin Y. M., Wang Y. Y., Yu I. S., Lin Y. W., Wang Y. H., Wu C. M., Pan H. A., Chao S. C., Yen P. H., Lin S. W., Kuo P.L. (2009): The expression level of septin12 is critical for spermiogenesis. Am J Pathol.;174(5):1857-68
Lindemann C. B., Lesich K. A. (2010): Flagellar and ciliary beating: the proven and the possible. J Cell Sci. 15;123(Pt 4):519-28.
Link J., Jahn D., Schmitt J., Göb E., Baar J., Ortega S., Benavente R., Alsheimer M. (2013): The meiotic nuclear lamina regulates chromosome dynamics and promotes efficient homologous recombination in the mouse. PLoS Genet.;9(1):e1003261
Link J., Leubner M., Schmitt J., Göb E., Benavente R., Jeang K. T., Xu R., Alsheimer M. (2014): Analysis of meiosis in SUN1 deficient mice reveals a distinct role of SUN2 in mammalian meiotic LINC complex formation and function. PLoS Genet 10(2): e1004099.
Maier W. M., Nussbaum G., Domenjoud L., Klemm U., Engel W. (1990): The lack of protamine 2 (P2) in boar and bull spermatozoa is due to mutations within the P2 gene. Nucleic Acids Res 18(5): 1249-1254.
Malone C. J., Fixsen W. D., Horvitz H. R., Han M. (1999): UNC-84 localizes to the nuclear envelope and is required for nuclear migration and anchoring during C. elegans development. Development 126(14): 3171-3181.
Freitas M. J., Vijayaraghavan S., Fardilha M., (2017): Signaling mechanisms in mammalian sperm motility, Biology of Reproduction, Volume 96, Issue 1, Pages 2–12.
Woop M., Schwab R. D., Lee H., Carter A. R. (2015): Optimizing Tethered Particle Motion to Measure DNA Compaction by Protamine. Biophysical Journal, VOLUME 108, ISSUE 2, SUPPLEMENT 1, 393A
Méjat A., Misteli T. (2010): LINC complexes in health and disease. Nucleus 1(1): 40-52.
Moir R. D., Montag-Lowy M., Goldman R. D. (1994): Dynamic properties of nuclear lamins: lamin B is associated with sites of DNA replication. J Cell Biol 125(6): 1201-1212.
Morimoto A., Shibuya H., Zhu X., Kim J., Ishiguro K., Han M., Watanabe Y. (2012): A conserved KASH domain protein associates with telomeres, SUN1, and dynactin during mammalian meiosis. J Cell Biol 198(2): 165-172.
Mostowy S., Cossart P. (2012): Septins: the fourth component of the cytoskeleton. Nat Rev Mol Cell Biol. 8;13(3):183-94.
Muciaccia B., Boitani C., Berloco B. P., Nudo F., Spadetta G., Stefanini M., de Rooij D. G., Vicini E. (2013): Novel stage classification of human spermatogenesis based on acrosome development. Biol Reprod.;89(3):60.
Mylonis I., Drosou V., Brancorsini S., Nikolakaki E., Sassone-Corsi P., Giannakouros T. (2004): Temporal association of protamine 1 with the inner nuclear membrane protein lamin B receptor during spermiogenesis. J Biol Chem.;279(12):11626-11631.
Oakberg E. F. (1956): A description of spermiogenesis in the mouse and its use in analysis of the cycle of the seminiferous epithelium and germ cell renewal. Am J Anat.;99(3):391-413.

Paci M., Elkhatib R., Longepied G., Bourgeois P., Ray P. F., Levy N., Mitchell M. J., Metzler-Guillemain C. (2018): The involvement of the nuclear lamina in human and rodent spermiogenesis: a systematic review. Basic Clin Androl. Jun 20;28:7

Paoli D., Gallo M., Rizzo F., Baldi E., Francavilla S., Lenzi A., Lombardo F., Gandini L. (2011): Mitochondrial membrane potential profile and its correlation with increasing sperm motility. Fertil Steril.;95(7):2315-9.

Pasch E., Link J., Beck C., Scheuerle S., Alsheimer M. (2015): The LINC complex component Sun4 plays a crucial role in sperm head formation and fertility. Biol Open 4(12): 1792-1802.

Pereira C. D., Serrano J. B., Martins F., da Cruz E., Silva O. A. B., Rebelo S. (2019): Nuclear envelope dynamics during mammalian spermatogenesis: new insights on male fertility. Biol Rev Camb Philos Soc.;94(4):1195-1219.

Pereira C. D., Serrano J. B., Martins F., da Cruz E. S. O. A. B., Rebelo S. (2019): Nuclear envelope dynamics during mammalian spermatogenesis: new insights on male fertility. Biol Rev Camb Philos Soc 94(4): 1195-1219.

Plant T. M., Zeleznik A. M. (2015): Knobil and Neill's Physiology of Reproduction, 4th edition, Academic Press, ISBN 978-0-12-397175-3

Ritagliati C., Luque G. M., Stival C., Baro Graf C.., Buffone M. G., Krapf D. (2018): Lysine acetylation modulates mouse sperm capacitation. Sci Rep 8, 13334.

Rogenhofer N., Dansranjavin T., Schorsch M., Spiess A., Wang H., von Schönfeldt V., Cappallo-Obermann H., Baukloh V., Yang H., Paradowska A., Chen B., Thaler C. J., Weidner W., Schuppe H. C., Steger K. (2013): The sperm protamine mRNA ratio as a clinical parameter to estimate the fertilizing potential of men taking part in an ART programme. Hum Reprod 28(4): 969-978.

Rogenhofer N., Ott J., Pilatz A., Wolf J., Thaler C. J., Windischbauer L., Schagdarsurengin U., Steger K., von Schönfeldt V. (2017): Unexplained recurrent miscarriages are associated with an aberrant sperm protamine mRNA content. Hum Reprod. 1;32(8):1574-1582.

Romrell L. J., Ross M. H. (1979) Characterization of Sertoli cell-germ cell junctional specializations in dissociated testicular cells. Anat Rec.;193(1):23-41.

Šanovec Ondřej. Buněčná odpověď na ribozomální stres, bakalářská práce Olomouc, 2019

Schneider S., Balbach M., Jan F. J., Fietz D., Nettersheim D., Jostes S., Schmidt R., Kressin M., Bergmann M., Wachten D., Steger K., Schorle H. (2016): Re-visiting the Protamine-2 locus: deletion, but not haploinsufficiency, renders male mice infertile. Sci Rep 6: 36764.

Schneider S., Shakeri F., Trötschel C., Arévalo L., Kruse A., Buness A., Poetsch A., Steger K., Schorle H. (2020): Protamine-2 Deficiency Initiates a Reactive Oxygen Species (ROS)-Mediated Destruction Cascade during Epididymal Sperm Maturation in Mice. Cells 9(8).

Schütz W., Alsheimer M., Ollinger R., Benavente R. (2005a): Nuclear envelope remodeling during mouse spermiogenesis: postmeiotic expression and redistribution of germline lamin B3. Exp Cell Res 307(2): 285-291.

Schütz W., Benavente R., Alsheimer M. (2005b): Dynamic properties of germ line-specific lamin B3: the role of the shortened rod domain. Eur J Cell Biol 84(7): 649-662.

Sen Gupta A., Sengupta K. (2017): Lamin B2 Modulates Nucleolar Morphology, Dynamics, and Function. Mol Cell Biol 37(24).

She Z. Y., Yu K. W., Wei Y. L., Zhong N., Lin Y. (2021): Kinesin-7 CENP-E regulates the formation and structural maintenance of the acrosome. Cell Tissue Res 383(3): 1167-1182.

Shen J., Chen W., Shao B., Qi Y., Xia Z., Wang F., Wang L., Guo X., Huang X., Sha J. (2014): Lamin A/C proteins in the spermatid acroplaxome are essential in mouse spermiogenesis. Reproduction.;148(5):479-87.

Shida T., Cueva J. G., Xu Z., Goodman M.B., Nachury M.V. (2010): The major alpha-tubulin K40 acetyltransferase alphaTAT1 promotes rapid ciliogenesis and efficient mechanosensation. Proc Natl Acad Sci U S A. 14;107(50):21517-22.

Soda T., Miyagawa Y., Ueda N., Takezawa K., Okuda H., Fukuhara S., Fujita K., Kiuchi H., Uemura M., Okamoto Y., Tsujimura A., Tanaka H., Nonomura N. (2017): Systematic characterization of human testis-specific actin capping protein β3 as a possible biomarker for male infertility. Hum Reprod.;32(3):514-522.

Starr D. A. (2011): KASH and SUN proteins. Curr Biol 21(11): R414-415.

Starr D. A., Fridolfsson H. N. (2010): Interactions between nuclei and the cytoskeleton are mediated by SUN-KASH nuclear-envelope bridges. Annu Rev Cell Dev Biol 26: 421-444.
Steger K. (1999): Transcriptional and translational regulation of gene expression in haploid spermatids. Anat Embryol (Berl) 199(6): 471-487.
Steger K., Failing K., Klonisch T., Behre H. M., Manning M., Weidner W., Hertle L., Bergmann M., Kliesch S. (2001): Round spermatids from infertile men exhibit decreased protamine-1 and 2 mRNA. Hum Reprod ;16:709–716.
Steger K., Wilhelm J., Konrad L., Stalf T., Greb R., Diemer T., Kliesch S., Bergmann M., Weidner W. (2008): Both protamine-1 to protamine-2 mRNA ratio and Bcl2 mRNA content in testicular spermatids and ejaculated spermatozoa discriminate between fertile and infertile men. Hum Reprod.;23(1):11-6.
Vergnes L., Péterfy M., Bergo M. O., Young S. G., Reue K. (2004): Lamin B1 is required for mouse development and nuclear integrity. Proc Natl Acad Sci U S A.13;101(28):10428-33.
Vester B., Smith A., Krohne G., Benavente R. (1993): Presence of a nuclear lamina in pachytene spermatocytes of the rat. J Cell Sci 104 (Pt 2): 557-563.
Visconti P. E., Galantino-Homer H., Ning X., Moore G. D., Valenzuela J. P., Jorgez C. J., Alvarez J. G., Kopf G. S. (1999a): Cholesterol efflux-mediated signal transduction in mammalian sperm. beta-cyclodextrins initiate transmembrane signaling leading to an increase in protein tyrosine phosphorylation and capacitation. J Biol Chem 274(5): 3235-3242.
Visconti P. E., Ning X., Fornés M. W., Alvarez J. G., Stein P., Connors S. A., Kopf G. S. (1999b): Cholesterol efflux-mediated signal transduction in mammalian sperm: cholesterol release signals an increase in protein tyrosine phosphorylation during mouse sperm capacitation. Dev Biol 214(2): 429-443.
Ward W. S., Coffey D. S. (1991): DNA packaging and organization in mammalian spermatozoa: comparison with somatic cells. Biol Reprod 44(4): 569-574.
Wykes S. M., Krawetz S. A. (2003): The structural organization of sperm chromatin. J Biol Chem 278(32): 29471-29477.
Xiong Z., Zhang H., Huang B., Liu Q., Wang Y., Shi D., Li X. (2018): Expression pattern of prohibitin, capping actin protein of muscle Z-line beta subunit and tektin-2 gene in Murrah buffalo sperm and its relationship with sperm motility. Asian-Australas J Anim Sci.;31(11):1729-1737.
Gruenbaum Y., Goldman R. D., Meyuhas R., Mills E., Margalit A., Fridkin A., Dayani Y., Prokocimer M., Enosh A., (2003): The nuclear lamina and its function in the nucleus, Int. Rev. Cytol. 226. 1 – 62.
Yanagimachi R. (2011): Mammalian Sperm Acrosome Reaction: Where Does It Begin Before Fertilization? Biology of Reproduction 85(1): 4-5.
Yang W-X., Sperry A. O. (2003): C-Terminal Kinesin Motor KIFC1 Participates in Acrosome Biogenesis and Vesicle Transport1. Biology of Reproduction 69(5): 1719-1729.
Yeh C. H., Kuo P. L., Wang Y. Y., Wu Y. Y., Chen M. F., Lin D. Y., Lai T.H., Chiang H.S., Lin Y. H. (2015): SEPT12/SPAG4/LAMINB1 complexes are required for maintaining the integrity of the nuclear envelope in postmeiotic male germ cells. PLoS One 10(3): e0120722.
Yeh C. H., Kuo P.L., Wang Y. Y., Wu Y. Y., Chen M. F., Lin D. Y., Lai T. H., Chiang H. S., Lin Y.H. (2015): SEPT12/SPAG4/LAMINB1 complexes are required for maintaining the integrity of the nuclear envelope in postmeiotic male germ cells. PLoS One. 16;10(3):e0120722.
Yeh C. H., Wang Y. Y., Wee S. K., Chen M. F., Chiang H. S., Kuo P. L., Lin Y. H. (2019): Testis-Specific SEPT12 Expression Affects SUN Protein Localization and is Involved in Mammalian Spermiogenesis. Int J Mol Sci. 7;20(5):1163.
Zakrzewski P., Rędowicz M. J., Buss F., Lenartowska M. (2020): Loss of myosin VI expression affects acrosome/acroplaxome complex morphology during mouse spermiogenesis†. Biol Reprod 103(3): 521-533.
Zhang Y., Yang L., Huang L., Liu G., Nie X., Zhang X., Xing X. (2021): SUN5 Interacting with Nesprin3 Plays an essential role in sperm head-to-tail linkage: Research on Sun5 gene knockout mice. Front Cell Dev Biol.;9:684826.
Zhi E., Li P., Chen H., Xu P., Zhu X., Zhu Z., He Z., Li Z. (2016): Decreased Expression of KIFC1 in Human Testes with Globozoospermic Defects. Genes 7(10): 75.

Zhu F., Wang F., Yang X., Zhang J., Wu H., Zhang Z., Zhang Z., He X., Zhou P., Wei Z., Gecz J., Cao Y. (2016): Biallelic SUN5 Mutations Cause Autosomal-Recessive Acephalic Spermatozoa Syndrome. Am J Hum Genet. 6;99(4):942-949.

10 Supplementary figures

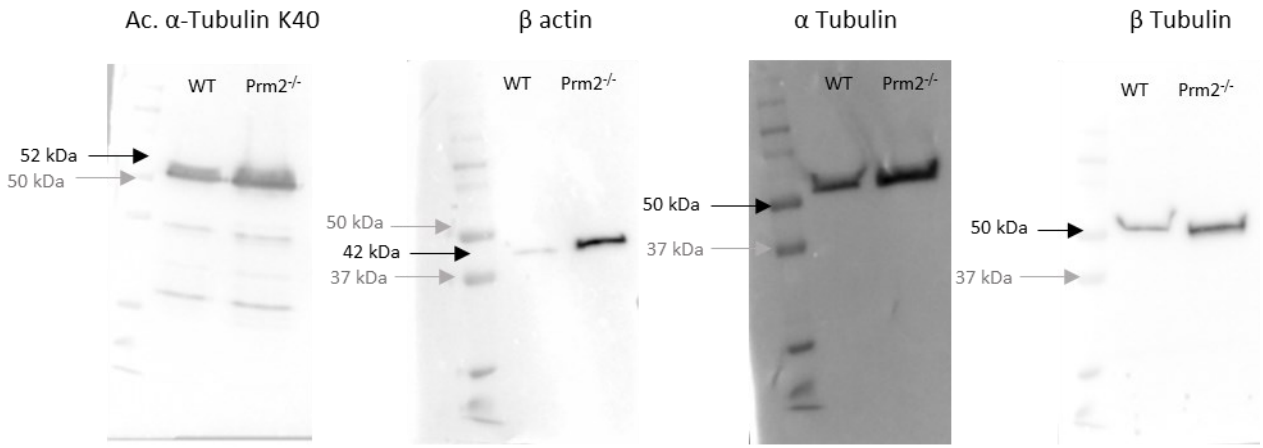

Supplementary figure 1: Whole membranes from Western blot. All samples, except α-tubulin acK40, showed only 1 specific band. α-tubulin acK40 showed some nonspecific signals in areas significantly different from its predicted size. (35 kDa and lower). Black arrows indicate the molecular weight of targeted proteins, grey arrows show the corresponding band on the protein marker.

Novel *in situ* volume imaging for studying spermatogenesis in 3D in Prm2 deficient mice

Sanovec, Ondrej [1] ; Ded, Lukas [1] ; Hubert Schorle [2] ; Steger, Klaus [3] ; Komrskova (Dvorakova-Hortova), Katerina [1,4]

[1] Laboratory of Reproductive Biology, Institute of Biotechnology of the Czech Academy of Sciences, BIOCEV, Vestec, Czech Republic.
[2] Institute of Pathology, Department of Developmental Pathology, University of Bonn Medical School, Bonn, Germany.
[3] Department of Urology, Pediatric Urology and Andrology, Section Molecular Andrology, Biomedical Research Center of the Justus-Liebig University, Giessen, Germany.
[4] Department of Zoology, Faculty of Science, Charles University, Prague 2, Czech Republic.

INTORDUCTION

Studying the tissue structure and histogenesis in 3D context is challenging but highly beneficial process. Contrary to classical approach of the physical tissue sectioning and subsequent imaging, it enables us to study the relationships of individual cellular and histological structures in their native context. Recent developments in the tissue clearing approaches and microscopic volume imaging/data processing enable the application of these methods also in the areas of developmental and reproductive biology.

In the present study, we focused on studying the LINC complex (Linker of Nucleoskeleton and Cytoskeleton) and its role in sperm head formation, sperm motility loss and its effects on nuclear composition in wild type and *Prm2* deficient mouse. Since The LINC complex is located within the sperm nuclear membrane, we hypothesized, that it represents the key for unravelling the link between the absence of the sperm nuclear protein protamine-2 and lack of motility in the sperm. We also targeted changes in tubulin acetylation patterns in *Prm2* KO sperm tail, as it was previously shown that increased tubulin acetylation positively corelates with reduced sperm motility.

HYPOTHESIS

- LINC complex represents the key for unravelling the link between the absence of Protamine 2 and lack of sperm motility.
- Pattern of α-tubulin acetylation at K40 is changed in Prm2 deficient sperm.
- Spermiogenesis is disrupted in *Prm2* deficient mouse leading to sperm with abnormally shaped head.

METHODS

- Immunofluorescence microscopy of mouse formalin-fixed paraffin-embedded (FFPE) testes to study localization of LINC complex through spermiogenesis.
- Immunofluorescence microscopy of mouse sperm to study changes in α-tubulin acetylation.
- Western blot to study changes in protein amount of acetylated α-tubulin.
- Development of novel protocol for microscopy sample preparation to study spermiogenesis in individual seminiferous tubules in 3D.

RESULTS

Here, we present optimized novel method for clearing, staining and imaging of mouse seminiferous tubules isolated from the testes without cardiac perfusion procedure. Our newly developed approach enables the high magnification and fine resolution axial imaging of the whole diameter of the seminiferous tubules with possible unlimited lateral length imaging. This knowledge was utilized to compare the spermiogenesis in wild type (WT) mouse and pathological spermiogenesis in *Prm2* deficient mouse. We have also examined localization of one component oft he LINC – SUN4 and its relationship with nuclear lamina. Other LINC components will follow .

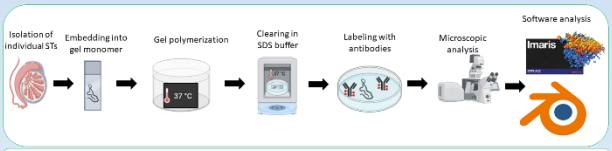

Fig. 1. Schematic representation of sample preparation and workflow.

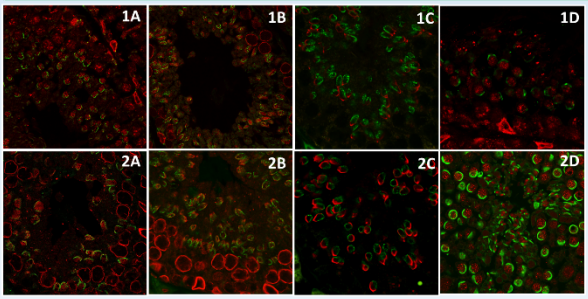

Fig. 2. Localization of LINC component SUN4 is not changed in *Prm2*$^{-/-}$ mouse compares to WT. **1)** *Prm2*$^{-/-}$, **2)** WT
A) SUN4 + Lamin B2, **B)** SUN4 + Lamin B2/3, **C)** SUN4 + PNA, **D)** PNA + Lamin B2/3

CONCLUSION

Classical approach such as immunohistochemistry of tissue sections didn't reveal any effect of *Prm2* deletion on nuclear lamina or SUN4, LINC component, localization and function during spermiogenesis (Fig. 2). Therefore, we focused on massive parallel imaging and developed new protocol for tissue samples preparation. Here we demonstrate brief protocol of sample preparation, with representative examples obtained using Lightsheet microscopy with examples of software postprocessing. During data processing, it was discovered that acrosome biogenesis in *Prm2* deficient mouse is disrupted (Fig. 5D). Moreover, patterns in α-tubulin acetylation but not protein quantity seems to be changed in *Prm2*$^{-/-}$ mouse. Our results show highly enriched α-tubulin acetylation in *Prm2*$^{-/-}$ sperm, where the signal was homogeneously distributed through whole sperm tail, compared to WT sperm, with acetylated α-tubulin located to principal and end piece of the tail.

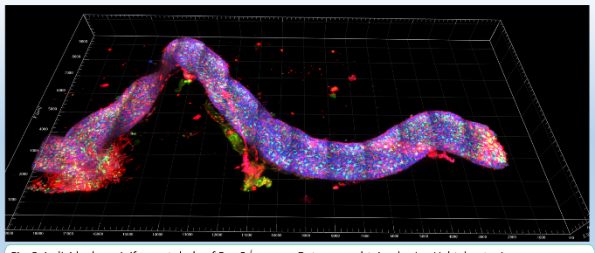

Fig. 3. Individual seminiferous tubule of Prm2$^{-/-}$ mouse. Data were obtained using Lightsheet microscopy.
Acetylated tubulin, Acrosome, DNA

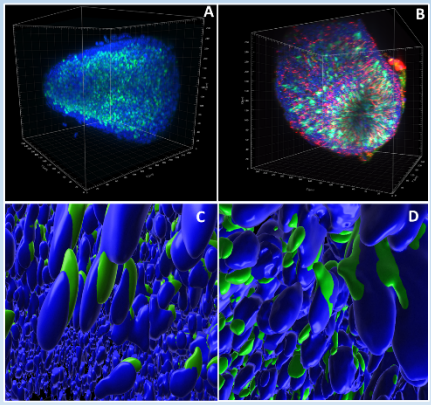

Fig. 4. Pathological acrosome development in Prm2-/- mouse studied by our newly developed protocol.
A) Individual seminiferous tubule of WT mouse, front-lateral view. **B)** Individual seminiferous tubule of Prm2-/- mouse, front view. **C, D** Image reconstruction by Imaris software. **C)** WT mouse, **D)** Prm2 -/- mouse.
Acetylated α-tubulin, Acrosome, DNA

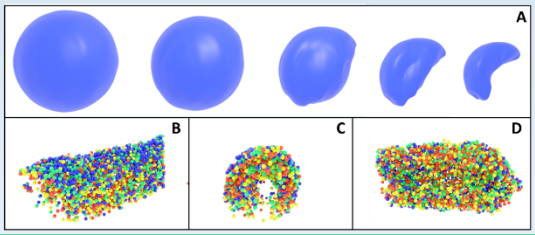

Fig. 5. **A)** Nuclear compaction and reshaping during spermiogenesisi. Computer simulation based on data obtained form microscopy. **B-D** Different cell populations visualization based on 5A. **B)** lateral view, **C)** front view, **D)** posterior to anterior view – optical section of middle lane of the seminiferous tubule.

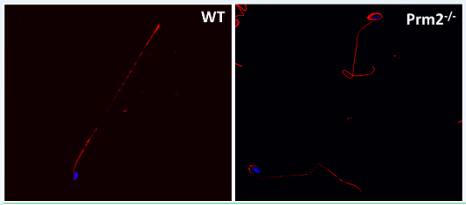

Fig. 6. Localization of Acetylated α-tubulin in mouse sperm. DNA.

Acknowledgment: This work was by GAČR: GC20-20217J, BIOCEV:CZ.1.05/1.1.00/02.0109) and by institutional grant RVO: 86652036, financially supported. Travel cost to the conference were partially covered by Nadace Nadání Hlohovských scholarship. Thank you for your support.

Supplementary figure 2: Poster presented on 54th annual meeting of Society for the Study of the Reproduction (December 2021, St. Louis, USA)